PART I. THE EFFECT OF DISSOLVED OZONE ON THE CORROSION BEHAVIOR OF STAINLESS STEELS IN ARTIFICIAL SEAWATER

W.E. Wyllie II and D.J. Duquette
Rensselaer Polytechnic Institute
Troy, NY 12180

PART II. THE EFFECT OF DISSOLVED OZONE ON THE CORROSION BEHAVIOR OF Ni-Cr-Mo ALLOYS IN ARTIFICIAL SEAWATER

B.E. Brown and D.J. Duquette
Rensselaer Polytechnic Institute
Troy, NY 12180

JANUARY 1997

Report No. 3 to the Office of Naval Research
Contract No. N00014-94-1-0093

TABLE OF CONTENTS

PART I. THE EFFECT OF DISSOLVED OZONE ON THE CORROSION BEHAVIOR OF STAINLESS STEELS IN ARTIFICIAL SEAWATER

PART I. LIST OF TABLES

PART I. LIST OF FIGURES

PART II. THE EFFECT OF DISSOLVED OZONE ON THE CORROSION BEHAVIOR OF Ni-Cr-Mo ALLOYS IN ARTIFICIAL SEAWATER

PART II. LIST OF TABLES

PART II. LIST OF FIGURES

THE EFFECT OF DISSOLVED OZONE ON THE CORROSION BEHAVIOR OF STAINLESS STEELS IN ARTIFICIAL SEAWATER

W.E. Wyllie II and D.J. Duquette
Rensselaer Polytechnic Institute
Materials Science & Engineering Department
Troy, New York 12180-3590

ABSTRACT

The corrosion resistance of austenitic stainless steels in artificial seawater containing 0.2 to 0.4 mg/L dissolved ozone was investigated. According to cyclic polarization data, UNS S30400 and S31600 stainless steels are resistant to pit initiation after 8 weeks exposure to ozonated artificial seawater. However, if crevices exist, crevice corrosion is more severe in ozonated vs. aerated artificial seawater. Maximum crevice corrosion penetration rates of 8 and 5 mm/y were recorded for UNS S30400 and S31600, respectively, in ozonated artificial seawater compared to only 0.4 to 0.5 mm/y under aerated conditions. Mixed potential analysis of anodic and cathodic polarization predicts crevice corrosion rates for UNS S31600 that are in excellent agreement with the immersion sample data. Highly alloyed Ni, Cr, Mo, and N-bearing austenitic stainless steels are resistant to crevice corrosion in aerated and ozonated artificial seawater. However, differential oxidation corrosion was observed between surfaces of high and low ozone concentration, leading to local transpassive dissolution manifested as surface etching and superficial intergranular corrosion. After 47 weeks exposure to ozonated artificial seawater, microscopic pitting was observed in crevices of high alloyed stainless steels. Although intergranular corrosion and microscopic pitting of highly alloyed stainless steels are not considered severe, these modes of corrosion warrant further investigation in the interest of corrosion resistance in long term (> 1 year) service under oxidizing conditions in seawater.

Keywords: austenitic stainless steel, biofouling, bromate, bromide, chlorine, corrosion control, crevice corrosion, cyclic polarization, intergranular corrosion, mixed potential, oxidizing biocide, ozone, seawater, stainless steel, transpassive corrosion

INTRODUCTION

Ozone Treatment

Application. A common problem in both fresh and seawater-cooled industrial heat exchange systems is biofouling and biofilm proliferation. Biological film growth can decrease the efficiency of heat transfer surfaces. Microbial activity in biofilms can lead to an insidious form of corrosion known

as microbiologically induced corrosion (MIC). Conventional methods of biological control include chlorine based chemical treatments of cooling waters. However, there is pressure by governmental agencies to minimize the release of environmentally hazardous byproducts of chlorine. Ozone is considered to be a safe, effective, and environmentally sound alternative to the chlorine based chemicals. Ozone is readily produced from oxygen or air via the corona discharge method in commonly available generation systems. Ozone eventually decomposes back to oxygen, so ozone treatment does not produce environmentally hazardous chlorinated organic byproducts. An industrial application of ozone treatment of fresh water is in cooling towers of power plants. The conversion from chlorine-based biocides to ozone treatment also is a consideration for seawater-cooled heat exchange systems of coastal power plants and naval vessels.

Biocidic action. The biocide action of ozone results from the oxidation of organic molecules in macro- and microbiological organisms. Videla and co-workers noted that 0.2 to 0.5 mg/L ozone for 10 to 15 minutes was effective to control aerobic biofilms.[1] However sessile bacteria were not completely removed by 0.15 mg/L ozone,[2] believed to be the result of the oxidation products of ozone with organics impeding the penetration of ozone into the underlying layers of the biofilm. It is possible that increased ozone concentrations, for instance 0.5 mg/L, combined with periodic flushing would remove the oxidation products and effectively control the biofilming. It should be noted that the treatment values cited above are for reference only. One must consider the degree of establishment of films (age, thickness) the ozone demand of the system, and the cooling water chemistry in specifying ozone treatment. Additionally, routine biological analysis should be performed in order to monitor the biocidal effectiveness of the treatment.

Ozone in Seawater

Ozone is one of the strongest oxidizers used in water treatment. Table I compares the reduction potentials in the standard state and at nominal conditions of seawater with the oxidant present.[3] Hypochlorous acid (HOCl) and hypobromous acid (HOBr) are the active biocidal chemicals in chlorinated and brominated water, respectively.

Bromide reactions. Ozone chemistry in seawater is complex, with the presence of oxidizable inorganic species such as bromide providing the greatest demand on ozone in artificial seawater. Research on ozonated seawater chemistry has shown that bromide is oxidized by ozone (eqn. 1) to hypobromite (OBr^-), in a manner similar to the oxidation of bromide by hypochlorite (ClO^-) to BrO^- in chlorinated waters.[4-7] Once formed by ozonation, the BrO^- can react again with ozone along a path that returns to Br^-, (eqn. 2) effectively creating a catalytic decomposition loop for molecular ozone.[8]

$$O_3 + Br^- \longrightarrow O_2 + BrO^- \qquad k_1 = 160\ M^{-1}s^{-1}\ (1)^9$$

$$O_3 + BrO^- \longrightarrow 2O_2 + Br^- \qquad k_2 = 330\ M^{-1}s^{-1}\ (2)^9$$

The hypobromite ion associates with H^+ ion and forms HOBr which is a very effective disinfectant.[10-12] Ozone also oxidizes BrO^- to form bromate (BrO_3^-):[7,9,13]

$$2O_3 + BrO^- \longrightarrow 2O_2 + BrO_3^- \qquad k_3 = 100\ M^{-1}s^{-1}\ (3)^9$$

As the pH increases or as bromide concentration decreases in ozonated solutions, it has been shown that the oxidation of BrO^- to BrO_3^- is predominant;[14,15] and all Br^- in seawater is effectively converted to BrO_3^- through exhaustive ozonation.[7] This is not surprising, as bromate is the stable bromine species at the oxidizing redox potential of ozone at alkaline pH ranges of the Pourbaix diagram.[16]

Monitoring ozone in seawater requires the use of techniques that are ozone-specific in the presence of other oxidants (e.g. HOCl and HOBr) and should be supplemented by the analysis of bromine species (Br^-, HOBr, BrO_3^-).[17]

Corrosivity. The corrosivity of ozone-bearing waters is not fully understood[18] due to contradicting results in fresh water research and limited work in saline solutions.[18-20] There is concern as to the effect of ozone on the corrosion behavior of alloys such as stainless steels used in the construction of seawater heat exchangers. The alloys included in the study are commonly available iron-chromium-nickel alloys, Type 304 stainless steel (UNS(1) S30400) and Type 316 stainless steel (UNS S31600), as well as higher chromium, nickel, molybdenum, and nitrogen-bearing austenitic stainless steels that are alloyed for seawater corrosion resistance. The higher alloyed grades are AL6XN®(2) (UNS N08367), 654SMO®(3) (UNS S32654), and Remanit 4565S®(4) (alloy 4565S).

Alloying Effects on Localized Corrosion Resistance

In order for stainless steels to resist localized corrosion in seawater, the alloy must resist pit initiation and also must maintain passivity in the reducing acidic environment that develops in a crevice. Increasing chromium tends to lower the critical current density (i_{crit}), passive current density (i_{pass}), and the primary passivation potential (E_{pp})[21] while increasing the breakdown potential (E_b), with the greatest increases in E_b seen in the 20 - 35 % Cr range in binary Fe-Cr alloys.[22] Nickel increases E_b[22] in Fe-Cr alloys and greatly improves the general corrosion resistance of Fe-Cr alloys.[23]

Adding molybdenum to Fe-Cr-Ni provides a marked increase in resistance to localized corrosion. In 25 wt.% Cr steels with 0 to 5 wt.% Mo, i_{crit} was reduced in 1 N H_2SO_4+ 1 N HCl and 3.5 and 5 % Mo alloys were resistant to pitting in HCl and $FeCl_2$ solutions.[24] In Fe-18Cr alloys, 2 to 8 % Mo resulted in marked decreases in i_{crit} and also shifted E_{pp} in the active direction.[25] It has been proposed that Mo confers resistance to dissolution in crevice solutions by forming a protective salt film.[26] Substantial chromium is required for the enhancement of crevice corrosion resistance by molybdenum to be realized.[27] Streicher's analysis[28] of multiple crevice assembly data from filtered seawater showed that alloys with high chromium contents (≥ 25 wt.% Cr) and at least 3.5 wt.% molybdenum were virtually immune. Factors that increased the crevice corrosion susceptibility were low chromium (≤ 20 wt.% Cr), substantial nickel (≥ 20 wt.% Ni) and copper.

Nitrogen has a very beneficial effect on the crevice corrosion behavior of austenitic stainless steels that already contain substantial Cr and Mo. Early studies showed that low carbon, high N, Mo, and Si were beneficial to pitting resistance.[29] Alloying with 0.07 to 0.35 % N increased breakdown potential in 18Cr-5Ni-10Mn steels.[30] The beneficial effects of N were reported to be even greater with Mo present.[31] It is interesting to note that, although Mn alone has a negative effect on localized corrosion resistance,[30] substantial Mn is required to dissolve N to concentrations above 0.35 wt.%. The resulting beneficial effects of high N with Mo tend to offset the negative effect of manganese.[27] A 20Cr-24Ni-6Mo with 0.4 wt.% N alloy was reported to be as resistant as nickel base alloy C-276 in acidified NaCl.[32] At 0.1 to 0.25 wt.%, nitrogen was shown to improve the resistance of 20Cr-24Ni-6Mo stainless steel to oxidizing chloride and reducing acid environments.[33]

---

(1) UNS numbers are listed in *Metals and Alloys in the Unified Numbering System*, published by the Society of Automotive Engineers (SAE) and co-sponsored by ASTM.
(2) Registered trademark of Allegheny Ludlum Steel.
(3) Registered trademark of Avesta Sheffield AB.
(4) Registered trademark of Thyssen Edelstahlwerke AG.

Corrosion Test Methods

The cyclic potentiodynamic polarization (CPP) technique, or simply "cyclic polarization" is a well documented test[34] used to study the susceptibility of a passive metal or alloy to localized corrosion in a specific environment. The typical parameters identified are the breakdown potential (E_b) where stable pitting occurs, and repassivation potential (E_{rp}) where the pitting ceases due to repassivation. changes resulting in active shifts in E_b and E_{rp} relative to E_{corr} increase the risk of pitting corrosion and crevice corrosion, respectively, while noble shifts in E_b and E_{rp} have the opposite effect. Large hysteresis is an indicator of high localized corrosion susceptibility.

Crevice corrosion can be studied by galvanic corrosion methods. Kain and Lee[35] studied crevice corrosion of UNS S31600 with crevice solutions similar to those of Oldfield and Sutton,[36] in which one test utilized a compartmentalized cell where the cathode and anode members are physically separated but galvanically coupled through a zero resistance ammeter. Kain and Lee showed that with pH of less than 1.1 the stainless steel behaved in an active manner. Above pH 1.1 the anodes became passivated in the anolyte, being polarized into a small passive range.

The anodic polarization in the simulated crevice solution, such as the deaerated 6 M chloride, pH 0.8 seawater solution used by Kain and Lee,[35] can be used to determine crevice corrosion rates through mixed potential analysis. A separate cathodic polarization curve measured in the bulk environment (e.g. aerated seawater) is superimposed on the anodic curve measured on a crevice-free sample in the simulated crevice solution. The intersection represents the crevice corrosion current for the theoretical galvanic couple. This technique has been used for corrosion resistant alloys in aerated and chlorinated seawater.[37,38] For complete assessment of the data, crevice corrosion rates calculated from the mixed potential analysis should be compared to crevice corrosion rates from of actual immersion tests.

Seawater Corrosion Behavior

Aerated seawater crevice corrosion rates. Lee and Money studied crevice corrosion multiple crevice assemblies in synthetic and natural seawater.[39] After 30 days at 25°C in synthetic seawater, UNS S30400 and S31600 exhibited maximum depths of attack of 0.11 and 0.08 mm, respectively, while in natural seawater, the maximum depths were 2.91 and 1.12 mm, respectively. At 50°C in synthetic seawater, the maximum depths of attack were only slightly higher than the 25°C results, and the differences between synthetic and natural seawater were very small. The presence of organics and biological activity were cited to explain the higher rates at 25°C in natural *versus* synthetic seawater, while the lower rate at 50°C is explained by the pasteurizing effect on the biological factors that enhanced crevice corrosion in natural seawater at 25°C.

In immersion tests using polymethylmethacrylate (PMMA) crevice washers, Kain reported a depth of penetration in UNS S31600 of 1.55 mm after 60 days in natural seawater, while UNS N08367 and S32654 were unattacked.[40] UNS S31600 assemblies with PMMA crevice washers corroded to depth ranges of 0.01 - 0.79 mm after 30 days in natural seawater while corrosion of N08367 assemblies were < 0.01 mm. Tube samples of N08367 exhibited an intergranular appearance, with maximum depths of < 0.01 mm, at the crevice formed between a rubber gland seal after 90 days in flowing natural seawater.[41] In two year exposure to natural and chlorinated seawater, UNS S32654 did not exhibit crevice attack under PMMA crevice formers, with and without soft polyvinyl chloride inserts,[42] however nickel base alloys 625 and C276 did show signs of crevice corrosion.

Effect of oxidizing biocides. Tests on 304L stainless steel (UNS S30403) in 0.5 N NaCl have shown more noble corrosion potentials with ozonation.[19] Cyclic polarization tests on UNS S30403

also indicated an increase in E_b with ozonation, indicating stabilization of the passive film and increased pitting resistance. However, at 0.2-0.4 mg/L ozone, the corrosion potential was equal or slightly noble to the repassivation potential (E_{rp}), indicating possible crevice corrosion susceptibility.[19] Cyclic polarization studies of S30403 in chlorinated 0.5 N NaCl (20 and 60 mg/L HOCl) showed noble shifts in E_{corr} and E_b, with E_{rp} active to E_{corr}. Cyclic polarization samples showed a lower number of pits but greater mean pit diameter for chlorinated compared to non-chlorinated conditions. Further work[18] on S30400 in artificial seawater found similar behavior, with E_{corr} and E_b shifting in the noble direction while E_{rp} was active to E_{corr} after 17 hours exposure to ozonated artificial seawater. In a 30 day test, a UNS S30400 sample with a PTFE(5) crevice washer showed lower pit density but deeper pit depth in ozonated versus aerated seawater.

In the literature described above, the passive film appeared to be stabilized during ozonation[18,19] or chlorination[43] due to the more oxidizing potential of the oxidizing biocide, and it is believed that the more noble cathodic regions coupled to the smaller anodic pit area resulted in a high driving force and a greater propagation rate. To supplement these conclusions, the kinetics of the oxidant reduction can also be considered. Ozone or HOCl reduction current densities that are higher than oxygen reduction current density would enhance the growth of the passive film, but at the same time would tend to drive higher localized dissolution rates at pits to which the oxidant reduction is coupled.

EXPERIMENTAL PROCEDURE

Samples

Table II shows the composition of the different alloys used in the test program. The weight loss and small cathode area crevice samples were 1.0x2.0 in. (2.5x5.1 cm) coupons cut from plate, in which a 0.38 in. (0.95 cm) diameter hole was machined. Three samples were used as weight loss samples, and the rest were used as crevice samples. Large cathode area crevice samples, measuring 1.5x3.0 in. (3.8x7.6 cm), were cut from sheet or plate stock, with a 0.38 in. (0.95 cm) diameter hole in the center. Plate samples were lapped with 9μm diamond abrasive to get a uniform flat surface. Wire samples were obtained as weld wire of various diameters. Only alloys UNS S30400, S31600, and N08367 were available for testing as wire electrochemical samples. Eight samples of each of the wire alloys were prepared for testing. Wire samples were annealed prior to testing; each wire was cut into 12 in. (30 cm) lengths for surface preparation. Both plate and wire were ground through 600 grit abrasive, rinsed with distilled water, ultrasonically cleaned in ultrasonic cleaning detergent solution made in distilled water, and finally rinsed twice with distilled water. All samples were dried with filtered compressed air immediately after cleaning. All samples were measured and weighed before attaching to the test fixtures.

Sample fixturing. A glass suspension rack was used in each 20 gallon (76 L) tank, consisting of removable 0.25 in. (0.63 cm) glass rods situated on a glass rack. The glass rack was custom fabricated from 0.4 in. (1 cm) diameter glass rod.

Three crevice-free weight loss samples of each alloy were supported through their holes on a glass rod, using PTFE tubing as spacers between the samples. Crevice samples were assembled between two PTFE multiple crevice washers. Each multiple crevice washer was 0.625 in. (1.59 cm) outer diameter x 0.25 in. (0.64 cm) inner diameter, with 12 crevice sites per washer, resulting a total of 24 sites per crevice sample. The sample and PTFE washers were clamped between Grade-2 titanium

(5) polytetrafluoroethylene

washers and secured with a 1/4-20 (0.25 in. diameter, 20 threads per inch) Grade-2 titanium bolt and nut. The portion of the multiple crevice PTFE washer which was in contact with the surface of the sample to form the tight crevice is designated the plateau. The region between the plateaus is termed the slot. The effective contact dimensions of a typical plateau were 0.15x0.32 cm. A PTFE thread was tied on one end to one of the PTFE multiple crevice washers used for each sample; the other end of the thread was tied to a PTFE O-ring to suspend from the glass support rod. To electrically insulate the sample from the titanium bolt, the bolt was initially wrapped with PTFE tape. The crevice samples were assembled while submerged in aerated artificial seawater, in order to minimize air pockets and to initiate wetting in the PTFE multiple crevice washers. The crevice assemblies were tightened with one and a quarter turns from finger tight. The resistance between the sample and the bolt was checked with a multimeter to ensure that there was no electrical contact between the sample and fixture. The small cathode area samples had an effective cathode/anode area ratio of 20/1; large area samples had an effective ratio of 48/1.

Wire samples were bent at approximately a 1.3 cm radius into a "J" such that a straight end extended out of the solution, while being supported on the other end by the glass rod. This "J" shape allowed corrosion potential data to be collected directly in the tank without removing the wire. The ends of the wire were not exposed to the solution to avoid preferential corrosion on the transverse wire sections.

Solutions

Ten tanks of artificial seawater were prepared by adding 1946 g of Forty Fathoms Bio-Crystals™(6) (Marinemix) to 56L of distilled water in each tank. Marinemix is formulated to produce artificial seawater that contains all of the inorganic components of natural seawater, in accordance with ASTM D 1141-90[44]. The tanks were used to conduct corrosion tests on five different alloy groups in a larger research program;[45] 2 tanks were used exclusively for stainless steels. The initial bromide concentrations were measured in accordance with a procedure described in a earlier report.[17,45] The exposure tanks were ozonated at a rate 1 SCFH [standard cubic feet per hour] (0.03 m^3/hr) of O_3/O_2 gas using fritted glass bubblers; aerated seawater control tanks were aerated at a rate of 1 SCFH (0.03 m^3/hr).

The ozonated artificial seawater tanks were pre-ozonated before samples were immersed. After sample immersion, residual ozone and bromine species concentrations were measured at the same intervals (2, 4, 8, 16, 26, and 47 weeks) at which samples were removed for testing. The residual ozone was measured using the Indigo Trisulfonate Method.[46,47] Bromide, hypohalite, and bromate concentrations were measured using the titration procedures described elsewhere.[17,45] In order to compensate for evaporation and to prevent build-up of byproducts in both the aerated and ozonated tanks, 6L of artificial seawater were changed out weekly and replaced with fresh solution.

Ozone Generation and Delivery

Ozone was produced using oxygen gas (95 wt.% O_2) in a corona discharge tube generator, resulting in a ozone/oxygen gas stream of approximately 3.5 wt.% O_3 in 90 -95 % O_2 (based on the generator manufacturer's specifications). Details of the ozone delivery system are found in an previous report.[45] Stainless steel, PTFE, glass, and Norprene®(7) tubing were used in the delivery system; only

(6) Trademark of Marine Enterprises, Inc.
(7) Registered trademark of Norton Performance Plastics Corp.

PTFE and glass tubing were used inside the tanks. Glass tube flowmeters were used to control the flow rate of ozonated gas to the tank.

Testing

Immersion samples. Tests were performed at 2, 4, 8, 16, 26, and 47 week intervals. Before any samples were removed from or tested in the tanks, the water chemistry was tested in accordance with the methods described at the beginning of this section. At each time interval, weight loss samples were removed, rinsed in distilled water and allowed to air dry before weighing. After weighing, the samples were photographed, replaced on the glass rod(s) and returned to the tank.

One large cathode area crevice sample and, at 4, 8, and 16 weeks, one small crevice area sample of each alloy was removed and rinsed in distilled water. The resistance between sample and crevice clamping fasteners was checked with a multimeter. The samples were then rinsed in distilled water again and allowed to air dry. The samples were then weighed, photographed, and stored in a dessicator.

After the weight loss and crevice samples were removed, one wire of each alloy was used to monitor corrosion potential and linear polarization resistance in the tank. One wire of each alloy was carefully removed from the tank for testing in a one-liter cell. The wire remained submerged while removing both the wire and tank solution in the one-liter cell. A coarse fritted glass bubbler was placed in the cell, bubbling either air or ozonated gas at a rate of 0.02 - 0.05 SCFH (0.0006 - 0.0015 m^3/h). This low flow rate was selected to approximate the ozone delivery rate per volume of solution as applied to the 56L tank volumes.

Electrochemistry. Steady state corrosion potential, linear polarization resistance, and cyclic polarization were then performed on the wire in the one-liter cell. Afterwards, the wire was removed from the cell and the submerged length of the wire recorded in order to calculate area for later calculations. The electrical instrumentation consisted of one EG&G PAR[8] Model 273 potentiostat and two EG&G PAR Model 173 potentiostats with Model 276 computer interface modules. The potentiostats were controlled with EG&G PAR software running on a personal computer.

Cyclic polarization (CPP) tests were conducted using ASTM G61-76[34] as a guide, with modifications. The cells were aerated or ozonated during the test. Scans of all wires were performed at a rate of 1V/hr. The scan rate was chosen based on a series of preliminary cyclic polarization tests at different scan rates in deaerated seawater. One V/hr was the upper limit at which slower rates did not cause significant changes in the critical parameters of breakdown potential or repassivation potential.

The parameters of the CPP began with the initial and final potential at -0.250 V versus the open circuit corrosion potential (OCP). The point at which the CPP curve reversed direction was controlled with a threshold current of 6 mA in order to maintain consistent test parameters for all tests. Preliminary testing showed that the potential range of interest for cyclic polarization varied greatly between aerated and ozonated conditions and between different alloys. This variability precluded the use of a vertex potential as the single variable controlling the potential scan reversal.

Compartmentalized cell tests. Compartmentalized cell tests were designed according to the procedure used by Kain.[35] The basic setup consisted of a UNS S31600 anode in a simulated crevice environment cell coupled to a large area flag cathode of N08367 in an artificial seawater bulk solution cell. The N08367 alloy was chosen because it is resistant to waterline corrosion attack. Based on preliminary data, cathodic reduction on austenitic stainless steels is not strongly composition-dependent and the use of UNS N08367 in place of UNS S31600 for a cathode is warranted. The

[8] EG&G Princeton Applied Research

samples were prepared with a 600 grit finish according to the sample procedure described previously. The cathode/anode area ratios ranged from 16.6/1 to 20.7/1.

The cathode cell contained artificial seawater under either aerated, ozonated, or oxygenated conditions. Ozonated cathode cells were ozonated for 1 week beforehand to achieve a steady state ozonated seawater chemistry close to the chemistry in the ozonated seawater exposure tanks. The one-liter cells were physically separated but ionically connected through an ionic cell bridge with fine fritted ceramic discs on each end. The ionic cell bridge was filled with the non-acidified anolyte solution. The samples were galvanically coupled through a zero resistance ammeter (ZRA) circuit in the potentiostat. A schematic diagram of the compartmentalized cell apparatus is shown in Figure 1.

A reference electrode and salt bridge combination was used to monitor the continuous couple potential. An uncoupled UNS N08367 electrode, a high impedance potentiometer, and a second reference electrode were used for periodic measurement during the 8-10 day test of the open circuit potential in the cathode cell. The pH of the anode and cathode cell solutions was measured before and after the test.

Simulated crevice solution (anolyte). The anolyte was prepared by adding 5.5 moles of sodium chloride (NaCl) to each liter of artificial seawater. Considering the chloride in the artificial seawater, the effective Cl^- concentration was 6M. The anolyte was acidified to pH 0.5 with hydrochloric acid (HCl). The pH of the anolyte was 0.42 measured one week after the solution was made. The anolyte composition was made based on the crevice solution Cl^- concentration and pH considered by Oldfield and Sutton[36,48] and which was used in later compartmentalized cell tests by Kain and Lee[35] in aerated seawater tests. The anolyte was chosen because it is at the saturation limit for chloride with the pH adjusted to be in the range of experimentally measured values for UNS S31600 stainless steel.[36,49,50] The anolyte was deaerated with high purity argon (99.99%) at a rate of 0.1 SCFH (0.003 m^3/hr) into the exhaust gas trap. One fritted glass bubbler and one 0.6 cm diameter glass tube were used to purge the cell with argon.

Mixed Potential Analysis

Potentiodynamic polarization. Potentiodynamic scans (PDS) data were generated in one-liter cells using ASTM G5-87 [51] as a guide. A scan rate of 0.6 V/hr was used, to be consistent with similar anodic polarization studies [35,36] for UNS S31600 stainless steel in aerated seawater. The initial potential was -0.100 V versus OCP for anodic polarization. Wire and plate samples of S31600 were used as the working electrode in separate anodic polarization curves, carried out in the simulated anolyte described above, deaerated with argon for 3 hours prior to the polarization. Cathodic polarization scans were performed on UNS N08367 wire electrodes in aerated, oxygenated, and ozonated seawater. The cathodic scan in ozonated seawater was conducted in the test cell using a wire sample that was exposed for 8 days at open circuit conditions. Preliminary cathodic scans were tested on wires that were exposed to aerated seawater for 3 hours and 26 weeks; aside from minor E_{corr} variations, there was no significant effect of time of exposure on the cathodic reduction curves. Oxygenated cathodic scans were performed using the 90-95% oxygen feed gas for the ozone generator, after exposure for 3 hours in the gas-saturated solution.

The current measured in the polarization tests was normalized to current density. The current density of the cathodic and anodic scans was then multiplied by the cathode/anode area ratio of 20/1 and displayed as current on the mixed potential diagram. The data was presented in this manner, rather than plotting the raw current values directly, because the cathode areas and anode areas varied from test to test.

Sample Analysis

Pit depths were measured using a light focusing, micrometer-equipped microscope. For each sample the deepest crevice pit of all crevice sites attacked is reported for the maximum depth of attack. Area of crevice attack was measured using an image analysis program on a computer.

RESULTS

Solutions

The initial bromide concentration of all tanks was in the range of 820-880 µM/L (65-70 mg/L). After 4 weeks exposure to ozone, the concentration of bromide and its byproducts reached stable values, with 93-95 % as BrO_3^-, 3-5 % as free Br^-, and 1-3 % as HOBr and BrO^- (% of total Br). The pH stabilized to approximately 8.2 in ozonated tanks for the duration of the experiment, once samples were immersed. The predominance of BrO_3^- is expected to occur as it is the stable brominated species at the potential range for ozonated seawater. The ozone concentration was maintained within 0.2 to 0.4 mg/L for the duration or the tests. Aerated artificial seawater tank pH values remained between 8.2 and 8.3 for the duration of the test.

General Corrosion

Although the effect of ozonation was to increase general corrosion rates by an order of magnitude over aerated artificial seawater rates, the absolute rates in ozonated seawater are not considered to be technologically significant. For example, the highest rate recorded for UNS S30400, is only 20 µm/y (0.8 mpy). General corrosion is not the damaging corrosion mechanism in seawater, rather crevice corrosion is the concern, as illustrated by the localization of corrosion of the weight loss samples at the support holes. In contrast to UNS S30400 and S31600, all of the highly alloyed stainless steels exhibited general corrosion rates of no more than 0.1 µm/y.

Open Circuit Corrosion Potential

Figure 2 displays the results of open circuit corrosion potential testing of stainless steel wires in the aerated and ozonated artificial seawater exposure tanks Figure 2 shows that the corrosion potential of the 3 stainless steel electrochemical samples exposed to ozonated artificial seawater was shifted in the noble direction with respect to the aerated corrosion potential. By 4 weeks exposure, the ozonated corrosion potential was 0.8 to 0.9 V higher than the aerated corrosion potential. Beyond 4 weeks, a steady corrosion potential of approximately 0.82 V_{SCE} was reached for all 3 alloys in ozonated seawater. The aerated potential varied between from -0.2 to 0.1 V_{SCE} for S30400 and S31600, while N08367 showed generally more active aerated potentials, between 0.0 and -0.4 V_{SCE}.

Cyclic Polarization

<u>UNS S30400.</u> Cyclic potentiodynamic polarization (CPP) experiments were performed on UNS S30400 wire samples at each test interval. The CPP test was conducted in one-liter test volumes, as described in the experimental section. Results for the 4 and 8 week test interval are shown in Figure 3 and 4, respectively.

The aerated artificial seawater CPP for both time intervals shows a large hysteresis loop, with a breakdown potential (E_b) and a repassivation potential (E_{rp}) of approximately 0.4 and 0.0 V_{SCE}, respectively. CPP scans in aerated artificial seawater caused large, subsurface, cavernous pits, 0.2 - 0.3 mm in diameter, to develop on the wire surfaces. The large hysteresis area and degree of pitting after 4 and 8 weeks in aerated artificial seawater was typical of the cyclic polarization data for UNS S30400 at all time intervals. The areas of the wire not subjected to the CPP, but exposed to the aerated open circuit potential conditions in the tank (due to a shallower depth of submersion in the one liter cell compared to the tank), were not pitted. This observation indicates that polarization of the wires noble to the breakdown potential initiated stable pits, but as expected, pitting does not occur at open circuit corrosion potential conditions active to the breakdown potential. However, the open circuit E_{corr} was noble to E_{rp}, indicating that any existing pits would have a tendency to grow.

The CPP results for UNS S30400 exposed to ozonated artificial seawater at 1, 2, and 4 weeks resulted in large hysteresis areas and large subsurface, undercutting pits, similar to the aerated counterparts. By 4 weeks exposure, the effects of the stronger oxidant were apparent, as seen by the 0.4 V noble shift in zero-current potential. A large hysteresis loop is evident, with the E_{rp} active to the zero current potential by greater than 0.1 V. Deep, narrow pits grew at and below the waterline during CPP testing. After 8 weeks, the polarization curve for UNS S30400 in ozonated seawater is much different from that at 4 weeks. The zero current potential is positioned at a noble potential in the oxygen evolution range. A small passive range is recorded from 1.00- 1.04 V_{SCE}. There is no hysteresis in the ozonated CPP at 8 weeks, with the forward and reverse curves tracking the same path. Pitting was not observed from the cyclic polarization. This cyclic polarization behavior was noted at all subsequent time intervals as well. However, at the original waterline from open circuit potential conditions in ozonated seawater, hemispherical pits were observed under the corrosion product.

UNS S31600. The results of CPP tests on UNS S31600 are shown in Figure 5, after 8 weeks exposure to aerated and ozonated seawater. These data are representative of the data from other time intervals as well. The wire sample tested in aerated seawater shows a primary passive region, a transpassive range at 0.5 to 0.7 V_{SCE}, and a narrow secondary passive range from 0.7 to 0.8 V_{SCE}. An anodic spike at 0.9 V indicates intermittent breakdown. Evidence of the breakdown process is noted in the hysteresis once the scan reverses. Partial repassivation "steps" are noted in the reverse curve before reaching the final repassivation potential at 0.3 V_{SCE}. Visual examination revealed that the breakdown occurred as large, hemispherical pits of approximately 0.6 mm in diameter at the waterline of the CPP test. This type of pitting was observed at other time periods as well. The repassivation behavior is unusual and is believed to be due to the waterline pit being partially repassivated in the course of the reverse scan. The area of the sample not subject to the CPP test, but exposed to the open circuit conditions in the aerated seawater tank, was not pitted. This shows that stable pits did not initiate at open circuit potentials active to the breakdown potential.

In contrast to the behavior of the aerated CPP test, the sample tested after 8 weeks in ozonated seawater did not show breakdown at the waterline or anywhere on the submerged surface. The CPP curve shown in Figure 5 shows no hysteresis and follows reversible gas electrode behavior similar to UNS S30400 stainless steel after 8 weeks exposure to ozonated artificial seawater. This cyclic polarization behavior has been observed in ozonated conditions at all other time intervals as well. The surfaces exposed to ozonated seawater appear to be passivated to the degree where waterline pitting cannot initiate. However, during open circuit exposure in ozonated seawater, small hemispherical pits were observed at the original waterline where green/black scale was attached.

The CPP waterline pitting in aerated seawater was observed at 1, 8, 16, and 47 weeks but it was not seen at 4 weeks, 26 weeks, or during any preliminary CPP tests in aerated seawater. There is a

variation of the difference potential (E_b - E_{rp}) in the aerated condition with time. However, based on visual examination of the samples, there is no correlation between the difference potential or hysteresis and the occurrence of waterline pitting. Additionally, identifying a clear E_b was difficult.

UNS N08367. Cyclic potentiodynamic polarization (CPP) experiments performed on UNS N08367 exposed for the test periods show distinct differences between aerated and ozonated seawater. The curves recorded in aerated and ozonated solution after 4 weeks in the respective solutions are presented in Figure 6.

The CPP curves for UNS N08367 in aerated artificial seawater at other time periods are essentially the same as that at 4 weeks exposure. As seen in Figure 6, the curve contains a primary passive range, a transpassive range (0.35 - 0.6 V_{SCE}), a secondary passive range (0.6 -0.9 V_{SCE}), and slight hysteresis evident at 1.1 V_{SCE}. The reverse curve follows the oxygen evolution curve back to a final zero-current potential at 0.7 V_{SCE} in the secondary passive range. The lack of significant hysteresis and the position of the breakdown and repassivation potentials indicates resistance to localized corrosion. Visual observation of the aerated CPP sample revealed no pitting on the free surfaces or at the waterline.

After 4 weeks in ozonated artificial seawater, the zero-current potential is shifted to 0.8 V_{SCE}, which is within the secondary passive range as defined on the aerated CPP curve. The forward scan intersects a narrow tertiary passive range, possibly due to the formation of NiO_2. A breakdown potential is noted at 1.12 V_{SCE}. and a hysteresis loop develops upon reversal of the scan. Visual examination of all CPP samples from ozonated seawater revealed small, hemispherical pits of approximately 100 μm in diameter on free surfaces. No pitting was noted on the surfaces of the sample exposed to the open circuit conditions in the ozonated seawater tank.

Pitting at highly oxidizing potentials- UNS N08367. In the aerated CPP tests conducted at 1 - 47 week time intervals, the cyclic polarization reversal was controlled by threshold current, as explained in the Experimental section. As such, the resulting CPP data under aerated conditions did not exceed 1.3 V while the ozonated tests consistently reached at least 1.35 V, due to the differences in the anodic curve path between aerated and ozonated tests. Although there is negligible hysteresis was noted, cyclic polarization to 1.4 V_{SCE} in one aerated artificial seawater test resulted in the formation of the small hemispherical pits.

Crevice Corrosion Damage

UNS S30400 and S31600 immersion samples. Figure 7, shown for UNS S31600, is illustrative of the type of the crevice attack that occurred on S30400 and S31600 samples exposed to aerated *versus* ozonated seawater. The incidence of crevice corrosion attack as a function of exposure time for both alloys is presented in Figure 8. Large volumes of red corrosion product were associated with the crevice corrosion in ozonated seawater and later identified as iron(III) oxide using energy dipersive spectroscopy (EDS) during scanning electron microscope (SEM) analysis.

The incidence of crevice corrosion as a function of exposure time is presented in Figure 8 for aerated and ozonated artificial seawater. Note that these data are from single samples where there are 24 possible sites for crevice corrosion per sample. The data in Figure 8 show that the number of sites initiated increased with time. The number of sites initiated for 4, 8, and 16 weeks exposure in ozonated artificial seawater did not show a strong direct dependence on the sample size.

The 4, 8, and 16 week crevice samples were analyzed for the true crevice area. Samples from later time periods (26, 47 weeks) were not subject to the analysis in order to keep the samples in the as-

corroded condition. The crevice sample weight loss was normalized to the crevice damage area and time. The crevice corrosion rates for the large cathode area samples were generally larger than rates for the small cathode area samples due to the larger cathodic current available to drive the crevice corrosion rate. The maximum crevice corrosion rates for aerated conditions were 156 μm/y for both UNS S30400 and S31600. The maximum rates for ozonated artificial seawater were 5700 and 2910 μm/y for UNS S30400 and S31600, respectively.

Table III lists the number of sites attacked and the maximum depth of attack at each time interval. The number of sites attacked does not generally increase with an increase in sample size (cathode/anode area ratio), however the maximum depth of attack is dependent on the sample size.

Compartmentalized cell tests. The results of compartmentalized cell zero resistance ammeter (ZRA) testing are presented in Figures 9 and 10. The uncoupled, open circuit anode potential of UNS S31600 for each of the three tests was between -0.37 and -0.40 V_{SCE} prior to the galvanic coupling. Upon coupling to the respective cathodes, the couple potentials increased only slightly to more noble potentials. Over the course of the test the couple potentials did not change by more than 30 mV from the open circuit potential of the uncoupled anode. The open circuit potential in artificial seawater is presented in Figure 9. These data were collected on an uncoupled electrode (N08367) in the cathode compartment while the flag cathode was galvanically coupled to the anode via the compartmentalized cell apparatus. The data indicate that the couple is under cathodic polarization control; the cathode of the couple is polarized very close to the open circuit potential of the anode.

The couple current expressed is normalized to current density at the anode is shown in Figure 10 for nominal cathode/anode area ratio of 20/1 using approximately 3.3 cm^2 anodes. The actual areas were measured to normalize the data to current density. The oxygenated test was expected to have a higher corrosion current because of a higher limiting current density associated with higher oxygen concentration. However, Figure 10 shows approximately the same current density for the oxygenated test compared to the aerated test. It is possible that the galvanic couple between anodic dissolution and oxygen reduction did not intersect the diffusion-limited concentration polarization region of the cathodic reduction curve for oxygen. In this case the effects of 4 times greater oxygen concentration would not be observed.

It should be noted that a tightly adherent brown surface film was present on the anodes after removal from the compartmentalized cell test. This film was darker for the ozonated cathode test compared to the aerated or oxygenated tests. The presence of the film may limit the couple current based on IR drops through the film layer.

The important difference between aerated and ozonated curves is the order of magnitude greater current at steady state conditions. The higher current translates directly to the higher kinetic driving force for crevice corrosion under ozonated compared to aerated conditions. The anode current densities are 5.4×10^{-6} and 4.2×10^{-5} A/cm^2 for aerated and ozonated cathode conditions, respectively.

Mixed potential analysis. Figure 11 presents the mixed potential analysis diagram for crevice corrosion of UNS S31600. The anodic polarization of UNS S31600 wire and plate in the simulated crevice solution is superimposed on the cathodic polarization of UNS N08367 stainless steel in aerated and ozonated artificial seawater. The anodic scan of the wire electrode (19 wt.% Cr) exhibited a large active-passive loop with a passive range that extends to approximately 0.3 V_{SCE}. The anodic scan for the plate electrode (16 wt.% Cr) had a higher i_{crit} in the active-passive loop, as is expected for the lower chromium content. The polarization scan for the plate electrode was terminated before pitting could occur at the edges in contact with the epoxy mount. The resulting scan shows a very limited passive range with a higher passive current density than the wire. The cathodic reduction in oxygenated seawater is virtually the same as the aerated curve; the only difference is observed as the 3 to 4 times

higher limiting current. The data is displayed as total current for a hypothetical, 20/1 cathode/anode area ratio galvanic couple to predict the galvanic current. The ozone reduction curve intersects the anodic curve in the active dissolution range at a current approximately ten times greater than that for the aerated or oxygenated cases. The mixed potential analysis in Figure 11 indicates that order of magnitude greater crevice corrosion rates will be expected for an active crevice on UNS S31600 stainless steel in ozonated artificial seawater compared to aerated artificial seawater. Using the effective 1 cm^2 of anode area, the corrosion current densities from Figure 11 are $4.85x10^{-5}$ and $5.25x10^{-4}$ A/cm^2, corresponding to rates of 512 and 5540 μm/y for aerated and ozonated conditions, respectively.

Comparison of crevice corrosion rates. The maximum rate of crevice corrosion for UNS S30400 and S31600 stainless steels from the different methods is presented in Table IV. The column for maximum crevice depth is based on the deepest crevice cavity and shortest time combination taken from Table III.

Highly Alloyed Stainless Steels

Sample appearance. Figures 12 shows representative crevice samples of UNS N08367 after exposure to aerated and ozonated artificial seawater. Note that UNS S32654 and alloy 4565S were nearly identical in appearance. These nitrogen alloyed, high chromium, molybdenum and nickel alloys all resisted the degree of crevice corrosion attack that occurred on the less resistant UNS S30400 and S31600 stainless steels under ozonated conditions, based on visual examination with a low power stereo microscope.

Coloration from oxide build up is visible in the slot regions between crevice plateaus on the ozonated samples; the aerated samples show virtually no effect of the crevice. The appearance of the crevice areas for these higher alloyed stainless steels is a green/red oxide surrounding the plateaus of the crevice, with a buildup of darker, thicker oxide in the center of the slot. Increased exposure to ozonated seawater results in increased corrosion, manifested as thickening and cracking of the oxide in the center of the slots. Samples from 4, 8, and 16 week exposure were stripped of the corrosion product and analyzed for localized attack, while samples from 47 weeks exposure were analyzed in the SEM with the corrosion product intact.

Black corrosion product/precipitate was found at the mouth of the slots. The black precipitate is similar in nature to that found in ozonated seawater exposure tanks containing other nickel-bearing alloys. Preliminary studies[45] revealed that calcium oxide and nickel chlorate hydrate were present in the precipitate collected from the tank which contained nickel-base alloy samples.

Microscopic analysis. The samples taken out of ozonated artificial seawater after 47 weeks exposure were analyzed in the SEM in the as-corroded condition. A rust red colored oxide/salt layer was analyzed, similar to that seen on all samples after 16 weeks exposure in ozonated artificial seawater. According to EDS data, this layer was found to be primarily sodium and chlorine with iron. The oxide/salt layer at the plateau/slot transition was found to be the same composition as the layer in the center of the slot. The oxide at the center of the slot of S32654 was found to be high in is molybdenum, iron and oxygen with lesser amounts of sodium, chlorine and potassium.

Microscopic pits were found in the plateau of UNS N08367, a greater number found close to the plateau/slot transition (crevice mouth). A typical pit is shown in Figure 13a. The pits are angular rather than round and are approximately 40 μm across the mouth. Figure 13b shows a similar small plateau pit found on the 47 week sample on UNS S32654 underneath a potassium-rich precipitate.

Microscopic Analysis - Intergranular Corrosion. As small pits and signs of intergranular corrosion were noted on SEM analysis of the 47 week ozonated samples of UNS N08367, UNS S32654, and Alloy 4565S, investigation into the corrosion under the oxide/salt films in slot regions was conducted. The slot region corrosion product was stripped off of the 16 week samples and the samples were examined under a light stereo microscope. Figure 14 a -c shows the intergranular corrosion typical of UNS S32654, UNS N08367, and 4565S after removal of oxide/salt films. Intergranular corrosion was typically surrounded by areas of etching.

Incidence of etching/intergranular corrosion. The incidence of etching and intergranular corrosion in slots for samples from 4, 8, and 16 week exposure to ozonated artificial seawater was tabulated in Table V. In general, etching in the slot regions was present on most samples. Intergranular corrosion was only associated with slot regions that also had been etched.

DISCUSSION

General Corrosion

The low general corrosion rates in ozonated seawater indicate that, at highly oxidizing potentials, the stainless steels are exhibiting secondary passivity. Using UNS N08367 as an example, the steady state corrosion potential in ozonated artificial seawater, 0.8 V_{SCE}, is in the range of secondary passivity, 0.6 to 0.9 V_{SCE}, as shown in Figure 6 in aerated artificial seawater.

The UNS N08367 alloy achieves the steady state ozonated potential more readily than UNS S31600 or S30400 by responding to the stronger oxidant as an inert electrode. The reduction of ozone readily polarizes UNS N08367 from the initial, non-ozonated condition to a mixed potential E_{corr} that corresponds to the secondary passive range. In contrast, under aerated conditions, Figure 5 shows instability for S31600 in the secondary passive range (0.5 to 0.9 V) and according to Figure 3, UNS S30400 is prone to breakdown noble to 0.5 V. Upon exposure to ozonated seawater, stable surface films on UNS S30400 and S31600 must develop over a long time as the electrodes are polarized from non-ozonated conditions to more noble potentials. Once stable secondary passivity is achieved on each alloy, E_{corr} is stable at 0.8 V_{SCE}.

The potential shift observed in Figure 2 on the stainless steels (+0.8 to +0.9 V) is approximately the same as the difference between the calculated half-cell redox potentials for ozonated *vs.* aerated seawater, $\Delta e = 1.55 - 0.73 = +0.82$ V. This correlation shows that the corrosion potential of the alloys in ozonated seawater is influenced strongly by the presence of ozone rather than oxygen. At the oxygen content in the feed gas (P_{O_2} = 0.90-0.95 atm), the calculated half-cell redox potential for oxygenated seawater is 0.75 V_{SHE}, only 0.02 V noble to the aerated seawater value. Accordingly, higher oxygen concentrations in ozonated seawater are not the cause of the corrosion potential shifts.

Pitting Corrosion

UNS S30400 and S31600 in aerated conditions. In contrast to the behavior of UNS S30400 in aerated conditions, a breakdown potential of UNS S31600 is not clearly identifiable. Although a single waterline pit grew in tests where significant hysteresis was observed, breakdown did not occur with a marked change in slope of the polarization curve. Rather, the polarization curve recorded only intermittent anodic spikes while continuing to record gradual increases in oxygen evolution and transpassive corrosion current.

The nature of pitting on UNS S31600 during CPP testing demonstrates that the alloy is not immune to localized corrosion in aerated seawater, although it is more resistant to pitting on free surfaces than UNS S30400, which pitted severely during every aerated CPP test. The pitting resistance is attributed to the presence of 2.4 wt.% molybdenum. However, a minimum of 3.5 wt.% Mo for crevice corrosion resistance found in the literature[28] is not met and UNS S31600 is susceptible to crevice corrosion. The susceptibility to crevice corrosion is clearly evident from the immersion samples; the waterline in CPP confirms this. The waterline is like a crevice. The meniscus formed by the variation in surface tension between the gas, liquid, and metal surface is a restricted volume which inhibits transfer of dissolved species to and from the waterline region. Evaporation at the meniscus leads to a salt deposit, under which crevice conditions prevail. During anodic polarization, localized passivity breakdown occurs in the aggressive environment. Metal dissolution (oxidation reaction) is accelerated by the anodic polarization which removes electrons from the waterline area.

Ozone passivation. After 4 and 8 weeks exposure in ozonated artificial seawater for UNS S31600 and S30400 stainless steel, respectively, the alloys were passivated sufficiently to resist pit initiation. No breakdown potential was observed, no pitting developed, and the surfaces acted as reversible gas electrodes. The pre exposure to ozone in artificial seawater passivated the surfaces of UNS S30400 and S31600. In the literature, pre-exposure to oxidizing biocide, or aging, was cited as a beneficial effect on a high chromium + molybdenum austenitic stainless steel. Bardal et al.[52] mentioned that previous exposure to chlorinated seawater enhanced the resistance of 254SMO®(9) (UNS S32254) to crevice initiation of compared to a freshly exposed sample. Compere et al.[53] attributed the aging, represented by noble potential shifts of the pitting potential, of S31603 in aerated natural seawater to enrichment of chromium in the passive film, based on surface analyses. It is possible that enrichment of chromium occurred in ozonated seawater to increase resistance to pit initiation of S30400 and S31600 after an initial exposure period of 4 to 8 weeks. However, surface composition profiles from the literature[19] do not show significant differences in the surface composition of UNS S30403 exposed to ozonated versus non-ozonated 0.5 N NaCl. Without additional surface analyses of the ozonated samples, the general conclusion is limited to stating that the surfaces were passivated by ozone in artificial seawater.

These data suggest that, for actively exposed surfaces, ozone stabilizes the passive film against pit initiation. The absence of hysteresis may be interpreted as resistance of the ozone-passivated surface to localized corrosion in general. Yet where a crevice exists from the outset, such as in the crevice samples, localized corrosion is clearly more severe in ozonated artificial seawater. On the stainless steel electrodes that were exposed to ozonated seawater, large hemispherical pits were observed at the original waterline that formed during open circuit potential (OCP) conditions. This pitting is not predictable from the cyclic polarization data in ozonated seawater. As described above for UNS S31600 in aerated cyclic polarization, the waterline behaves like a crevice, where crevice conditions exist in the restricted volume of the meniscus and under the salt layer that forms via evaporation. The oxidizing potentials (0.8 V_{SCE}) in the bulk ozonated seawater polarize the surface in the waterline above the local breakdown potential, causing pitting. This observation is in accord with the crevice sample results which show serious crevice corrosion after only 2 weeks exposure.

UNS N08367. The pitting observed in the CPP testing in ozonated artificial seawater is not believed to be indicative of pitting in the open circuit condition. This conclusion is supported by the absence of pitting on samples after exposure to ozonated seawater at open circuit conditions. The pitting potential was found in an oxidizing potential range, 1.3 - 1.4 V_{SCE}, which is 0.5 to 0.6 V noble to

(9) Registered trademark of Avesta Sheffield AB

the open circuit potential in ozonated artificial seawater. The occurrence of pitting may be due to local dissolution of molybdenum.[54] Molybdenum is an active metal that does not form a passive film with a wide range of stability and is likely to dissolve at the highly oxidizing potentials achieved during the cyclic polarization.

The occurrence pitting of UNS N08367 is independent of aeration or ozonation, but the hysteresis associated with the pitting in CPP tests was greater in ozonated than in aerated seawater. This indicates that the presence of ozone hindered the repassivation of pits that were initiated. However, as pitting was only observed at potentials 0.5 - 0.6 V noble to E_{corr}, pitting is not considered significant for open circuit exposures in ozonated seawater.

Crevice Corrosion - UNS S30400 and S31600

If the data in Table III and Figure 8 are considered, the number of sites attacked does not generally increase with an increase in sample size (cathode/anode area ratio), however the maximum depth of attack is dependent on the sample size. These data suggest that the driving force for initiation is not linked to the cathodic current available per crevice area,, but the crevice corrosion propagation rate is controlled by the cathodic reduction rate to which it is galvanically coupled.

The data in Figure 8 indicate that crevice initiation continues with time independent of prior initiation and growth. The data indicate that the crevice initiation is a stochastic process, independent of a prior occurrence. If the initiation process was dependent upon the available cathodic reduction current, existing crevice corrosion would tend to bias against initiation and there would not be increasing numbers of sites attacked with increasing exposure time.

Crevice corrosion electrochemical tests. The compartmentalized cell results in Figure 10 reflect the order of magnitude greater corrosion rates under ozonated conditions. However, the compartmentalized cell ZRA test absolute current densities are lower than those predicted by the mixed potential analysis. It is possible that the anode became passive in the anolyte prior to and during the test. Kain and Lee[35,55] noted that in anolytes more aggressive than the critical crevice solution, (i.e. lower pH and higher [Cl^-]) the anode in a compartmentalized cell test could be anodically protected through polarization into the small passive range. Additionally, a tightly adherent brown surface film was present on the anodes as a result of the ZRA tests. This film could have acted as a barrier to dissolution; the IR drop through the film would limit the dissolution current to lower current densities.

When the mixed potential analysis electrochemical tests are considered, two results are apparent. The anodic polarization curve of UNS S31600 in the simulated crevice solution is in agreement with literature data.[35] The mixed potential analysis in Figure 11 indicates that order of magnitude greater crevice corrosion rates will be expected for an active crevice on UNS S31600 stainless steel in ozonated artificial seawater compared to aerated artificial seawater. The higher rates are due to ozone rather than oxygen (at 90 - 95 wt.%) in ozonated artificial seawater; aerated and oxygenated conditions are shown to drive virtually identical crevice corrosion rates. At a 20/1 cathode/anode area ratio, the predicted corrosion rates are 0.5 and 6 mm/y for aerated and ozonated artificial seawater, respectively. These values are in very good agreement with the maximum crevice depth of attack values, presented in Table IV.

Comparison of crevice corrosion rates. The maximum rate of crevice corrosion for S30400 and S31600 stainless steels from the different methods is presented in Table IV. As expected, UNS S31600 is somewhat more resistant to crevice dissolution than S30400 due to the presence of 2.5 wt.% Mo. However, the crevice corrosion rates are very high for both alloys and would prohibit their application in ozonated seawater where crevices exist. Utilizing mixed potential analysis as a method

for predicting crevice corrosion, rates calculated from this technique for UNS S31600 are in excellent agreement with crevice weight loss- and maximum depth of attack-based values.

Artificial *vs.* natural seawater crevice corrosion rates. Lee and Money[39] reported crevice corrosion rates of 1.35 and 0.97 mm/y for S30400 and S31600, respectively, in aerated artificial seawater. These data are comparable to the aerated crevice corrosion rates in the present work. However, natural seawater crevice corrosion rates are typically higher than those in artificial seawater. The 14 to 26 times increase in crevice corrosion rate from artificial to natural seawater reported by Lee and Money was attributed in a general sense to the "organic and biological components in natural seawater."[39] The maximum depth-based crevice corrosion rates for ozonated artificial seawater in the present study, 5 -8 mm/y, are on the order of those in aerated natural seawater found in the literature (in mm/y calculated from maximum depth of attack) for S30400 - 6.5, [56] 9,[57] 36[39] and for S31600 - 4.1,[56] 13.6,[39] 9.4,[40] 9.7.[41] The cited literature data are scattered, apparently due to variables such as seawater flow, chemistry, temperature, sample cathode/anode area ratio, surface finish of metal and crevice former, and term of exposure. According to the literature data, the biological factors in aerated natural seawater drive crevice corrosion rates at least an order of magnitude higher than those observed in artificial seawater. The literature data also indicate that the driving force for crevice corrosion in natural seawater is on the order of the driving force in ozonated artificial seawater. An interesting area for future work would compare the effect of ozonation and aeration in natural seawater on the crevice corrosion behavior.

High Alloyed Stainless Steels

Incidence of slot corrosion - N08367, S32654, alloy 4565S. Slot etching and intergranular corrosion were observed at the mouth of the crevice former facing the slot, in the center of the slot, and also on UNS N08367 electrochemical samples at the waterline which formed from open circuit exposure. Etching is the most prevalent result of differential oxidation corrosion, while intergranular corrosion appears to be a more aggressive form of etching corrosion.

The tendency for etching to occur is not strongly dependent on the alloy or the duration of exposure in ozonated artificial seawater, although etching and intergranular corrosion occurred to the greatest degree for UNS S32654, followed by UNS N08367 and Alloy 4565S. This trend is in decreasing order of Cr and Mo content, suggesting that the etching and intergranular corrosion is related to the amount of these elements present.

Differential oxidation/transpassive dissolution mechanism. Because of the geometric size of the slot, the migration of dissolved species into and out of the slot is expected to be limited, resulting in low ozone concentration in the slot relative to the bulk solution. The differential oxidation cell operates by ozone reduction on free surfaces in the bulk solution coupled to an anodic oxygen evolution and transpassive dissolution in the slot. Oxygen evolution and transpassive corrosion lowers the pH in the slot, and chloride ions migrate into the slot to maintain the charge neutrality. The coupling between ozonated, secondary passive free surfaces and the ozone-depleted, transpassive slots can be represented by mixed potential curves, shown in Figure 15. The cathodic curve is taken from the reverse curve of a CPP diagram for UNS N08367 after 4 weeks in ozonated artificial seawater, while the anodic curve is from the parallel test under aerated seawater conditions. A 10/1 cathode/anode ratio is used to illustrate the galvanic couple. The cathodic curve for ozone reduction intersects the non-ozonated (aerated) curve in the transpassive region.

It has been shown for nickel alloys in non-aggressive nitrate and chlorate solutions at potentials noble to the oxygen evolution potential, the passive film breaks down gradually. Oxygen evolution

occurs concurrently with transpassive metal dissolution, by a proposed mechanism where surface sites alternate between oxygen evolution and metal dissolution. After prolonged exposure to these conditions, a uniformly etched surface texture results.[58] Transpassive dissolution of nickel occurs as Ni^{3+} in the oxygen evolution range.[59] Transpassive corrosion of chromium is well-known,[23,60] with the dissolution of chromate ion (CrO_4^{2-}). Molybdenum also dissolves in a similar manner to form the molybdate ion (MoO_4^{2-}).[16] Because Cr and Mo are readily dissolved transpassively, alloys of the highest Cr and Mo content would be expected to exhibit transpassive corrosion.

For the high Ni, Cr, Mo alloys in the present study, the concurrent transpassive dissolution and oxygen evolution occurs in the slots, resulting in the etched surface appearance. The intergranular corrosion indicates that the grain boundaries are preferred sites for dissolution as opposed to oxygen evolution.

Grain boundary corrosion. Literature regarding the intergranular corrosion by chromate in non-sensitized stainless steels indicates that silicon or phosphorus segregated to the grain boundaries is a promoting factor.[61] However, electron microprobe line scans across grain boundaries[62] indicated no increases in silicon or phosphorus nor any depletion of any of the major alloying element at the grain boundary of UNS N08367. Alternatively, monolayer segregation of Si and/or P may have occurred so that the compositional variation across the grain boundary was below the resolution of the electron microprobe. The cause of intergranular corrosion could be the result of thermal grain boundary sensitization, however this is unlikely. All highly alloyed steels in the present study contain less than 0.03 wt.% carbon and have been developed to resist the sensitization reaction in fabrication. The grain boundary corrosion observed in the slot regions of crevice samples exposed to ozonated seawater may be explained by grain boundary etching.

On surfaces undergoing transpassive corrosion, grain boundaries were attacked in addition to the general etching. The grain boundaries are corroded preferentially due to their increased energy compared to the grain faces. Orientation mismatch between adjacent grains in a polycrystalline solid results in an array of dislocations situated in the boundary. The strain energy of each dislocation contributes to the overall grain boundary energy.[63] The higher energy state of the grain boundary lowers the activation energy for metal ion dissolution and the grain boundary preferentially corrodes while oxygen evolution occurs on the grain face. Moreover, the discontinuity in surface energy at the grain boundary can create local variations in the passive film integrity, resulting in lesser resistance to dissolution.

Waterline corrosion in cyclic polarization. Many of the UNS N08367 wires tested in ozonated seawater exhibited light intergranular corrosion and etching at the waterline that formed during open circuit conditions. The intergranular corrosion of wires at the waterline from open circuit conditions occurs in accordance with the differential oxidation and transpassive dissolution mechanism described above. The meniscus volume, depleted of ozone, becomes the anode to the cathodic free surface of the submerged wire. Corrosion progresses in the meniscus analogous to the slot regions of crevice samples. In the case of waterline corrosion resulting from cyclic polarization, the mechanism is the same, with an accelerating effect of the anodic polarization which draws electrons away from the anode.

Microscopic pitting in crevice plateaus. Microscopic pitting was observed in SEM images in the crevice plateau near the crevice mouth in high alloyed stainless steels after 47 weeks exposure to ozonated artificial seawater. Based on observations of the 47 week samples only, the data suggest that the propensity of microscopic pitting in the crevice is higher with high Ni, low Cr, higher Cu, and low

N. The microscopic pitting, although not a severe form of corrosion for the highly alloyed stainless steels, should be investigated for the long-term effects in an ozonated system.

CONCLUSIONS

- The corrosion resistance of austenitic stainless steels in artificial seawater containing 0.2 to 0.4 mg/L dissolved ozone was investigated. In continuously ozonated artificial seawater the oxidizing power of the solution is controlled by ozone rather than oxygen in the feed gas.

- Based on electrochemical measurements, exposure to ozonated artificial seawater results in secondary passive behavior for austenitic stainless steels. In this condition UNS S30400 and S31600 stainless steels are more resistant to pit initiation than after exposure to aerated artificial seawater for the same time duration. However, if crevices exist, crevice corrosion is more severe on UNS S30400 and S31600 in ozonated compared to aerated artificial seawater.

- Crevice corrosion rates are an order of magnitude higher in ozonated compared to aerated artificial seawater. Maximum rates of attack of 8 and 5 mm/y were recorded for UNS S30400 and S31600, respectively, in ozonated artificial seawater. In comparison, rates of 0.4 to 0.5 mm/y were measured in aerated artificial seawater.

- Mixed potential analysis predicts crevice corrosion rates for UNS S31600 that are in excellent agreement with the immersion sample data, using cathodic polarization curves measured in aerated and ozonated artificial seawater and anodic polarization curves recorded in a simulated crevice anolyte.

- Highly alloyed nickel, chromium, molybdenum and nitrogen-bearing austenitic stainless steels are resistant to crevice corrosion in aerated and ozonated artificial seawater. Differential oxidation cell corrosion was noted under ozonated conditions between free surfaces (high ozone concentration) and slots between crevice plateaus (low ozone concentration) where solution access is limited. Differential oxidation leads to surface etching and in the most aggressive instances, superficial intergranular corrosion. The etching and intergranular corrosion appear to be the result of transpassive dissolution in the slot region.

- After 47 weeks exposure to ozonated artificial seawater, microscopic pitting was observed in crevice plateau near the crevice mouth in high alloyed stainless steels. Visual observations suggest that microscopic pitting susceptibility is greatest in alloys with high Ni, high Cu, low Cr, and low N. Although differential oxidation corrosion and microscopic pitting of highly alloyed stainless steels is not considered to be severe in the current study, these modes of corrosion warrant further investigation in the interest of corrosion resistance in extended service under oxidizing seawater conditions.

ACKNOWLEDGEMENTS

The authors wish to acknowledge the financial support of the Office of Naval Research under Contract N00014-94-1-0093, monitored by Dr. A.J. Sedriks, and the donation of materials from Allegheny Ludlum Steel and Rolled Alloys Inc.

REFERENCES

1. H. A. Videla, M. R. Viera, P. S. Guiamet, M. F. L. de Mele and J. C. S. Alais, "Combined Action of Oxidizing Biocides for Controlling Biofilms and MIC," Corrosion/94, Paper No. 260, (Houston, TX: NACE, 1994).
2. H. A. Videla, M. R. Viera, P. S. Guiamet, M. F. L. de Mele and J. C. S. Alais, "Effect of Dissolved Ozone on the Passive Behavior of Heat Exchanger Structural Materials. Biocidal Efficacy on Bacterial Biofilms," Corrosion/95, Paper No. 199, (Houston, TX: NACE, 1995).
3. A. J. Bard and L. R. Faulkner, Electrochemical Methods: Fundamentals and Applications, (New York, New York: John Wiley & Sons, 1980).
4. P. M. Williams, R. J. Baldwin and K. J. Robertson, Journal of Water Research, 12, (1978) p. 385.
5. W. J. Blogoslawski, L. Farrell, R. Garceau and P. Derrig, "Production of Oxidants in Ozonized Sea Water," Proceedings of the Second International Symposium on Ozone Technology, (Ozone Press, 1976).
6. P. Pichet and C. Hurtubise, "Proceedings of the Second International Symposium on Ozone Technology," Symposium on Ozone Technology, (International Ozone Institute, 1976).
7. E. A. Crecelius, J. Fish Res. Board Canada, 36, (1979) p. 1006.
8. J. Hoigné and H. Bader, Water Research, 17, (1983a) p. 173.
9. W. R. Haag and J. Hoigné, J. Environ. Sci. Technol., 17, (1983a) p. 261.
10. R. P. Rice, "Fundamental Aspects of Ozone Chemistry in Recirculating Cooling Water Systems," Corrosion/91, Paper No. 205 (Houston, TX: NACE, 1991).
11. P. K. Mitchell, Pool & Spa News, April 15 (1985) p. 128.
12. W. R. Haag, J. Hoigné and H. Bader, Water Research, 18, (1984) p. 1125.
13. L. B. Richardson, D. T. Burton, G. R. Helz and J. C. Rhoderick, Water Research, 15, (1981) p. 1067.
14. J. J. Keaffaber, C. J. Costen and W. G. Ham, "Redox Chemistry of Closed Ozonation Systems: Modeling Bromine and other Redox Active Species," The Use of Ozone in Aquatic Systems, 1, (The International Ozone Association, 1992).
15. U. von Gunten and J. Hoigné, J. Water SRT--Aqua, 41, (1992) p. 229.
16. M. Pourbaix, Atlas of Electrochemical Equilibria in Aqueous Solutions, (Houston, TX: National Association of Corrosion Engineers, 1974)
17. W. E. Wyllie II, B. E. Brown and D. J. Duquette, "Ozone in Seawater I. Chemistry, II. Corrosion of Metals," Corrosion/95, Paper no. 269, (Houston, TX: NACE, 1995).
18. B. E. Brown and D. J. Duquette, "A Review of the Effects of Dissolved Ozone on the Corrosion Behavior of Metals and Alloys," Corrosion/94, Paper No. 486 (Houston, TX: NACE, 1994).
19. H. H. Lu and D. J. Duquette, Corrosion, 46, (1990) p. 843.
20. B. E. Brown, H. H. Lu and D. J. Duquette, Corrosion, 48, (1992) p. 970.

21. M. S. Walker and L. C. Rowe, Corrosion, 25, (1969) p. 47.

22. J. Horvath and H. H. Uhlig, J. Electrochemical Society, 115, (1968) p. 791.

23. H. H. Uhlig and R. W. Revie, Corrosion and Corrosion Control, (New York: John Wiley & Sons, 1985)

24. E. A. Lislovs and A. P. Bond, J. Electrochemical Society, 118, (1971) p. 22.

25. M. B. Rockel, Corrosion, 29, (1973) p. 393.

26. A. J. Sedriks, Corrosion of Stainless Steels, (New York, NY: John Wiley & Sons, Inc, 1979)

27. A. J. Sedriks, Corrosion, 42, (1986) p. 376.

28. M. A. Streicher, Materials Performance, 22, May (1983) p. 37.

29. M. A. Streicher, J. Electrochemical Society, 103, (1956) p. 375.

30. M. Janik-Czakor, E. Lunarska and Z. Szklarska-Smialowska, Corrosion, 31, (1975) p. 394.

31. M. J. Coleman and K. R. Pirt, Brit. Corros. J., 12, (1977) p. 236.

32. R. Bandy and D. V. Rooyen, Corrosion, 39, (1983) p. 227.

33. J. R. Kearns and H. E. Deverell, Materials Performance, 26, June (1987) p. 18.

34. ASTM G 61-86, "Standard Test Method for Conducting Cyclic Polarization Measurements for Localized Corrosion Susceptibility of Iron-, Nickel-, or Cobalt-Based Alloys," Annual Book of ASTM Standards, (Philadelphia, PA: ASTM, 1994)

35. R. M. Kain and T. S. Lee, "Recent Developments in Test methods for Investigating Crevice Corrosion," Laboratory Corrosion Tests and Standards, ASTM STP 866, G. S. Haynes and R. Baboian, ed. (Philadelphia, PA: ASTM, 1985) p. 299-323.

36. J. W. Oldfield and W. H. Sutton, Brit. Corros. J., 13, (1978) p. 104.

37. B. A. Shaw, P. J. Moran and P. Gartland, "Crevice Corrosion of a Nickel-Based Superalloy in Natural and Chlorinated Seawater," 12th International Corrosion Congress, (Houston, TX: NACE, 1993).

38. R. S. Lillard, M. P. Jurinski and J. R. Scully, Corrosion, 50, (1994) p. 251.

39. T. S. Lee and K. L. Money, Materials Performance, 23, Aug. (1984) p. 28.

40. R. M. Kain, "Seawater Testing to Assess the Crevice Corrosion Resistance of Stainless Steels and Related Alloys," 12th International Corrosion Congress, (Houston, TX: NACE, 1993).

41. R. M. Kain, B. Weber and W. L. Adamson, "Localized and General Corrosion Resistance of Candidate Metallic Materials For RO-Membrane Cartridges," Corrosion/95, Paper No. 268, (Houston, TX: NACE, 1995).

42. J. W. Oldfield, "Corrosion Initiation and Propagation of Nickel Base Alloys in Severe Sea Water Applications," Corrosion/95, Paper No. 266, (Houston, TX: NACE, 1995).

43. H. S. Lu and D. J. Duquette, Corrosion, 46, (1990) p. 994.

44. ASTM D 1141-90, "Standard Specification for Substitute Ocean Water," Annual Book of ASTM Standards, (Philadelphia, PA: ASTM, 1990)

45. W. E. Wyllie II, B. E. Brown and D. J. Duquette, "Interim Results On The Corrosion Behavior of Engineering Alloys in Ozonated Artificial Seawater," Office of Naval Research (Arlington, VA), End of Year Report No. 2, Contract No. N00014-94-1-0093, March 1996.

46. H. Bader and J. Hoigné, Water Research, 15, (1981) p. 449.

47. H. Bader and J. Hoigne, "Colorimetric Method for the Measurement of Aqueous Ozone based on the Decolorization of Indigo Derivatives," Ozonation Manual for Water and Wastewater Treatment, W. J. Masschelein, ed. (Chichester: John Wiley & Sons, 1982) p. 169-172.

48. J. W. Oldfield and W. H. Sutton, Brit. Corros. J., 13, (1978) p. 13.

49. T. Suzuki, M. Yamabe and Y. Kitamura, Corrosion, 29, (1973) p. 18.

50. J. Mankowski and Z. Szklarska-Smialowska, Corrosion Science, 15, (1975) p. 493.

51. ASTM G 5-87, "Standard Reference Test Method For Making Potentiostatic and Potentiodynamic Anodic Polarization Measurements," Annual Book of ASTM Standards, (Philadelphia, PA: ASTM, 1994)

52. E. Bardal, J. M. Drugli and P. O. Gartland, Corrosion Science, 35, (1993) p. 257.

53. C. Compere, P. Jaffre and D. Festy, Corrosion, 52, (1996) p. 496.

54. M. Johnson, Allegheny Ludlum Steel Corp., Personal Communication, March 1996.

55. R. M. Kain, T. S. Lee and J. W. Oldfield, "Use of Electrochemical Techniques for the Study of Crevice Corrosion in Natural Sea Water," Electrochemical Techniques for Corrosion Engineering, R. Baboian, ed. (Houston, TX: NACE, 1986) p. 261.

56. T. S. Lee, "A Method for Quantifying the Initiation and Propagation Stages of Crevice Corrosion," Electrochemical Corrosion Testing, ASTM STP 727, (Philadelphia, PA: ASTM, 1981) p. 43.

57. D. B. Anderson, "Statistical Aspects of Crevice Corrosion in Seawater," Galvanic and Pitting Corrosion - Field and Laboratory Studies, ASTM STP 576, Baboian, France, Rowe and Rynewicz, ed. (Philadelphia, PA: ASTM, 1976) p. 231-242.

58. D. Landolt, "Transpassivity," Passivity of Metals, R. P. Frankenthal and J. Kruger, ed. (Princeton, NJ: The Electrochemical Society, 1978) p. 484.

59. N. Sato and G. Okamoto, J. Electrochemical Society, 110, (1963) p. 605.

60. H. Kaesche, Metallic Corrosion, (Houston, TX: NACE, 1985)

61. J. S. Armijo, Corrosion, 24, (1968) p. 24.

62. W. E. Wyllie II, Ph.D. thesis, Rensselaer Polytechnic Institute, 1996.

63. R. E. Reed-Hill, Physical Metallurgy Principles (2nd Edition), (Monterey, CA: Brooks Cole Engineering, 1973) 219.

Table I. Reduction potentials of oxidants present in ozonated seawater.

Redox Couple	e^o (V_{SHE})	Nominal conditions in artificial seawater, pH 8.2	e (V_{SHE}) at nominal conditions
O_3/O_2	2.08	Ozonated, $p(O_3)$ = 0.024 atm	1.55
$HOCl/Cl^-$	1.48	Chlorinated, [HOCl] = 25 mg/l	1.15
$HOBr/Br^-$	1.33	Brominated, [HOBr] = 25 mg/l	1.08
O_2/OH^-	1.23	Oxygenated, $p(O_2)$ = 0.95 atm	0.75
O_2/OH^-	1.23	Aerated, $p(O_2)$ = 0.2 atm	0.73

Table II. Chemical composition (wt.%) based on mill analyses of stainless steel samples used for seawater immersion tests. S and L refer to small, 1.0x2.0 in. (2.5x5.1 cm) large, 1.5x3.0 in. (3.8x7.6 cm) plate samples, respectively.

	C	Cr	Fe	Mn	Mo	Ni	P	S	Si	Other
S30400 (S, L)	0.06	18.1	bal.	1.83	-	8.03	0.034	0.004	0.46	
S30400 (wire)	0.05	18.51	bal.	1.7	-	8.1	0.03	0.02	0.05	
316 SS (S)	0.057	16.56	bal.	1.67	2.44	11.84	0.033	0.015	0.66	
S31600 (L)	0.045	16.42	bal.	1.77	2.09	10.21	0.028	0.011	0.46	0.31 Cu, 0.038 N, 0.15 Co
S31600 (wire)	0.05	19.51	bal.	1.80	2.11	11.23	0.013	0.01	0.35	0.032 N
N08367 (S)	0.02	20.30	bal.	0.52	6.25	23.93	0.026	0.000	0.39	0.27 Cu, 0.24 N
N08367 (L)	0.015	20.48	bal.	0.34	6.23	23.90	0.021	0.000	0.38	0.24 Cu, 0.24 N
N08367 (wire)	0.020	20.45	bal.	0.30	6.19	23.68	0.015	0.001	0.34	0.09 Cu, 0.21 N
N08367 (sheet)	0.012	20.87	bal.	0.38	6.24	24.01	0.025	0.001	0.55	0.23 Cu, 0.22 N
S32654 (S, L)	0.016	24.40	bal.	3.65	7.26	21.9	0.017	0.000	0.26	0.44 Cu, 0.528 N
4565S (S, L)	0.022	23.57	bal.	5.57	4.2	17.65	0.018	<0.003	0.19	0.48 N, 0.04 Nb

Table III. Incidence of crevice attack and maximum depth of attack in multiple crevice samples for S30400 and S31600 stainless steels as a function of exposure time in aerated and ozonated seawater, from single sample data.

	4 WEEKS		8 WEEKS		16 WEEKS	
	A	O	A	O	A	O
S30400 (S)	0 0.0	3 0.460	0 0.0	4 0.343	0 0.0	8 0.513
S30400 (L)	1 0.030	3 0.595	0 0.0	2 0.508	0 0.0	11 0.816
S31600 (S)	1 0.037	3 0.185	0 0.0	8 0.266	2 0.044	12 0.421
S31600 (L)	0 0.0	3 0.361	1 0.039	6 0.693	0 0.0	6 0.970

A - Aerated, O - Ozonated S - small cathode area; L - large cathode area
Top value - # sites attacked (24 possible)
Lower Value - Max. depth of attack (mm), ± 0.005 mm (A), ± 0.020 mm (O)

Table IV. Maximum crevice corrosion rates (μm/y) of stainless steels in aerated and ozonated artificial seawater predicted from different test methods.
(Uncertainty values are listed as ± below each value)

Alloy/ environment	Crevice samples (weight loss)	Maximum crevice depth	Mixed potential analysis
S30400 aerated	**156** ±70	**390** ±65	–
S30400 ozonated	**5720** ±2570	**7740** ±260	–
S31600 aerated	**156** ±51	**481** ±65	**512** ±230
S31600 ozonated	**2910** ±1310	**4500** ±260	**5540** ±2490

Table V. Incidence of etching and intergranular corrosion in slots of multiple crevice samples for high-alloyed stainless steels as a function of exposure time in ozonated seawater. Aerated samples were unaffected.

(single sample data at each time period)

	4 WEEKS		8 WEEKS		16 WEEKS	
	A	O	A	O	A	O
N08367 (S)	—	0 0	—	0 0	—	3 0
N08367 (L)	—	4 2	—	4 0	—	9 2
S32654 (S)	—	5 0	—	6 1	—	8 1
S32654 (L)	—	7 0	—	8 0	—	11 4
4565S (S)	—	5 0	—	4 0	—	5 0
4565S (L)	—	11 1	—	1 0	—	6 0

A - Aerated, O - Ozonated; S - small cathode area; L - large cathode area
Top value - # Slots etched (24 possible)
Lower Value - # of etched slots with intergranular corrosion

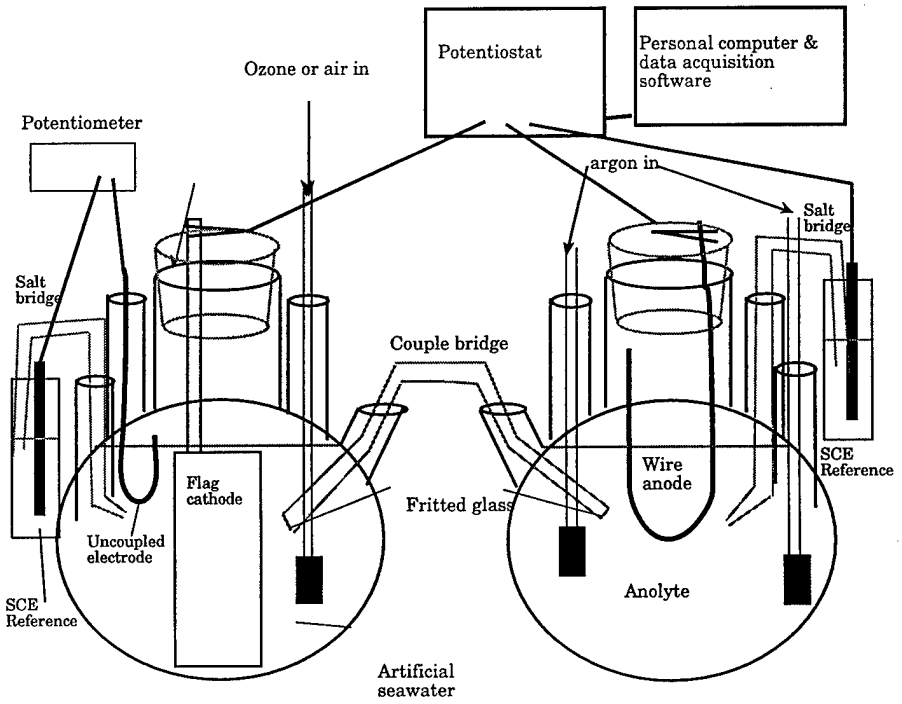

Figure 1. Schematic illustration of compartmentalized cell apparatus, where the potentiostat is used as a zero resistance ammeter (ZRA).

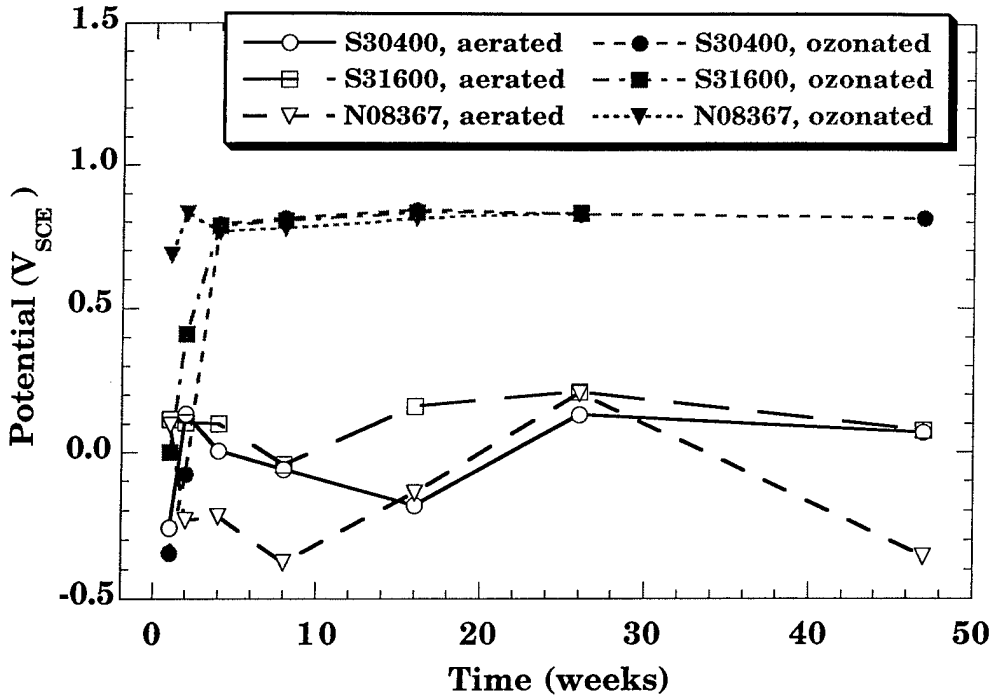

Figure 2. Open circuit corrosion potential of stainless steels in artificial seawater under aerated and ozonated conditions as a function of exposure time

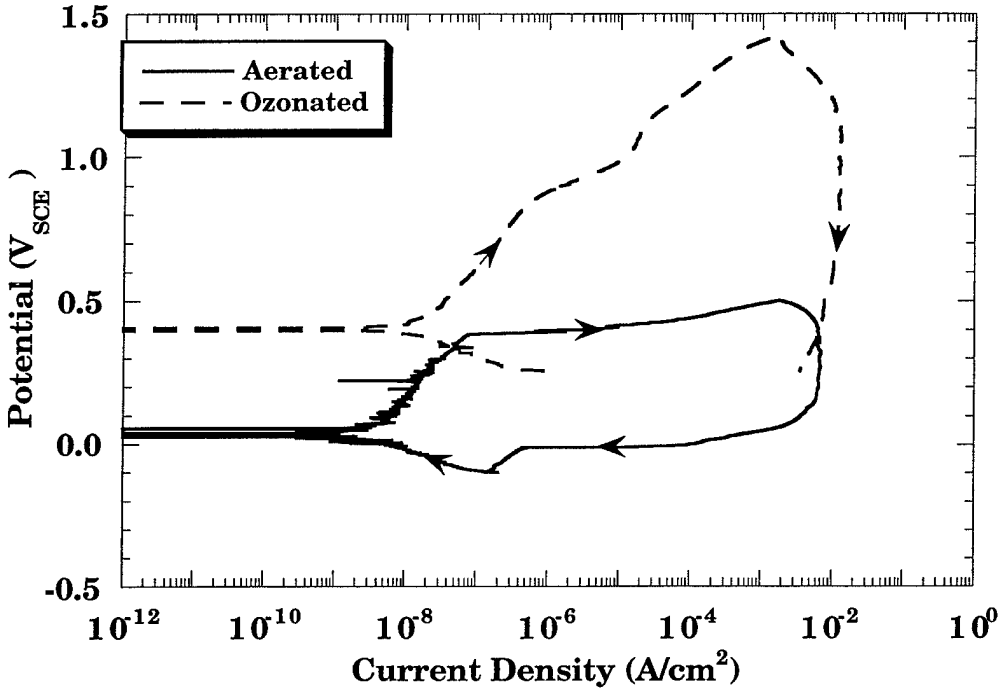

Figure 3. Cyclic polarization curves for UNS S30400 stainless steel after exposure to aerated and ozonated artificial seawater for 4 weeks. (Scan rate = 1 V/hr)

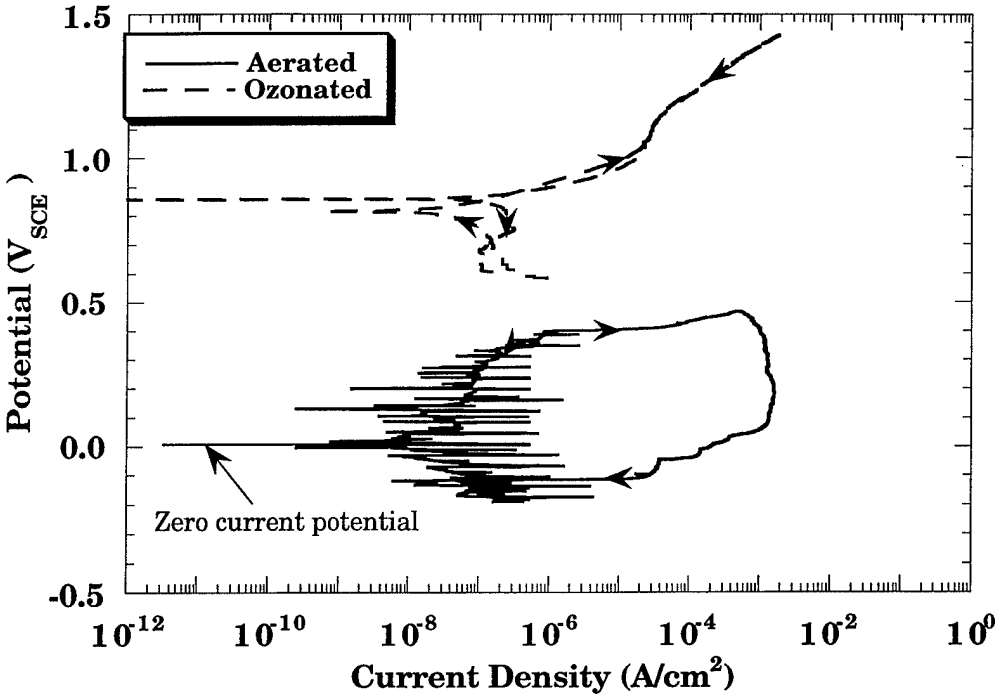

Figure 4. Cyclic polarization curves for UNS S30400 stainless steel after exposure to aerated and ozonated artificial seawater for 8 weeks. (Scan rate = 1 V/hr)

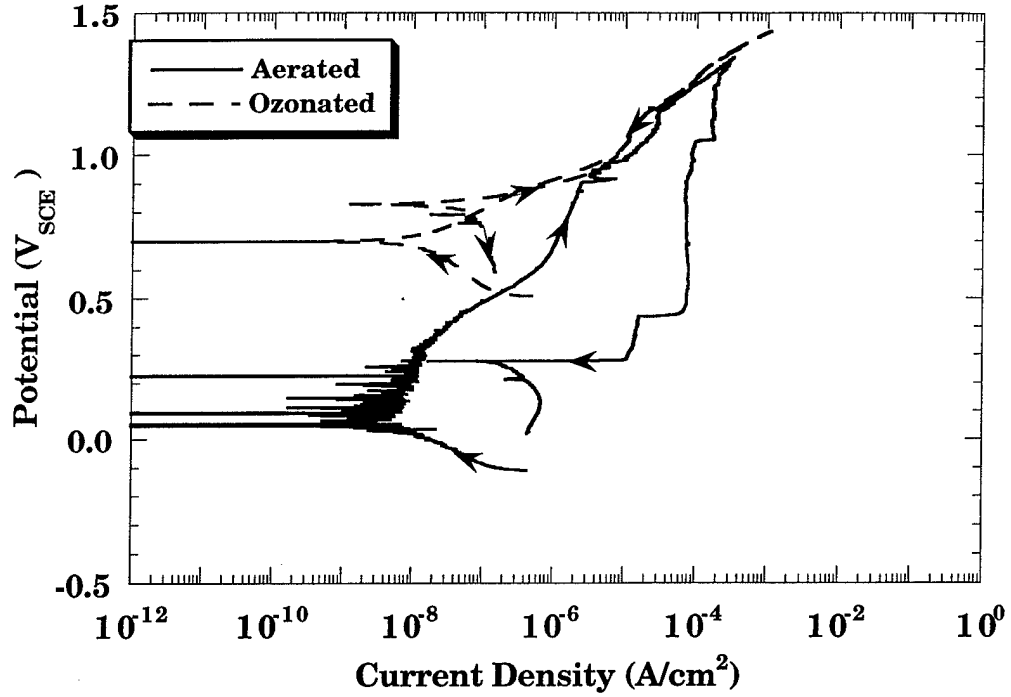

Figure 5. Cyclic polarization curves for UNS S31600 stainless steel after exposure to aerated and ozonated artificial seawater for 8 weeks. (Scan rate = 1 V/hr)

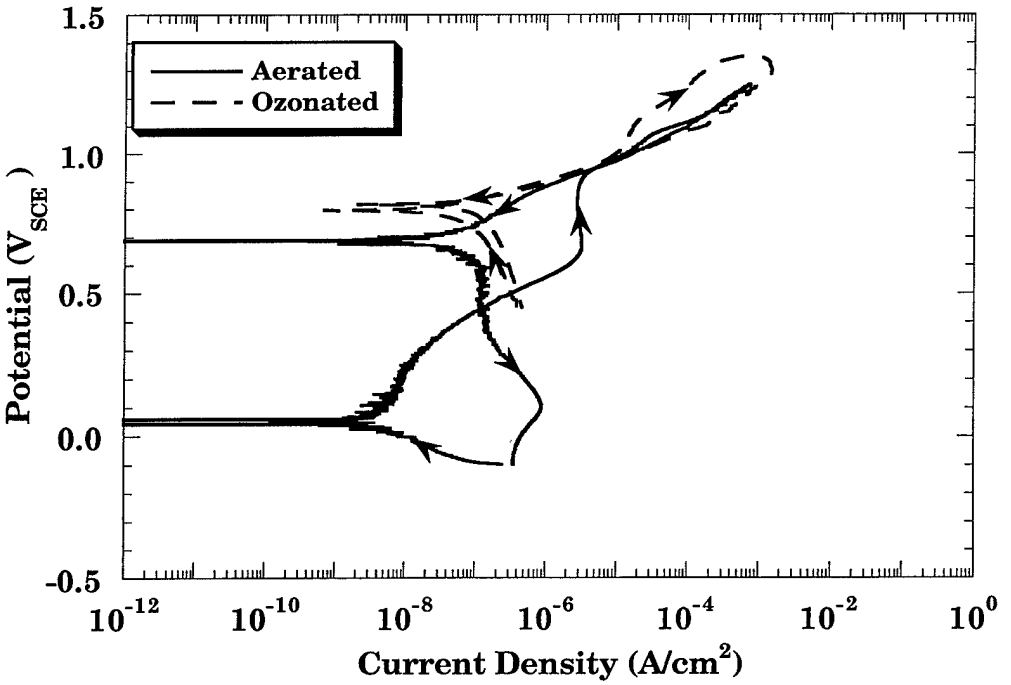

Figure 6. Comparison of polarization curves of UNS N08367 stainless steel exposed to aerated and ozonated artificial seawater for 4 weeks.

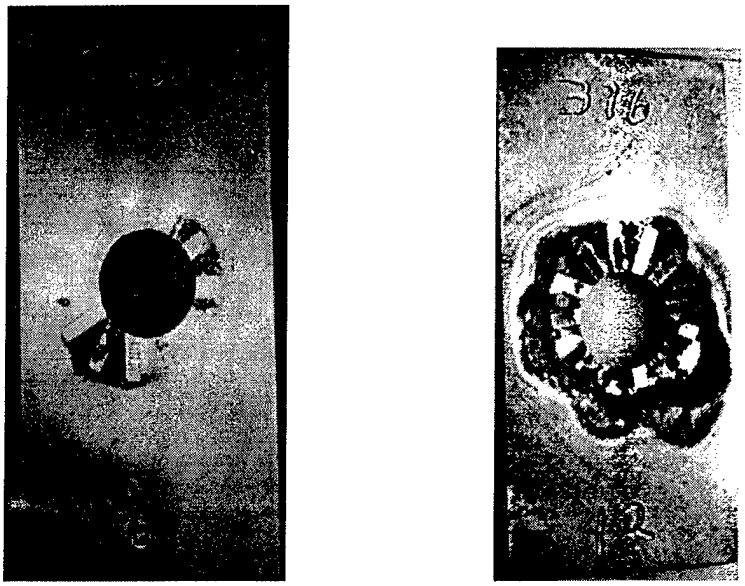

Figure 7. Small UNS S31600 samples, 1.0x2.0 in. (2.5x5.1 cm) exposed for 16 weeks: (a) aerated artificial seawater, (b) ozonated artificial seawater. Appearance of UNS S30400 was similar in nature.

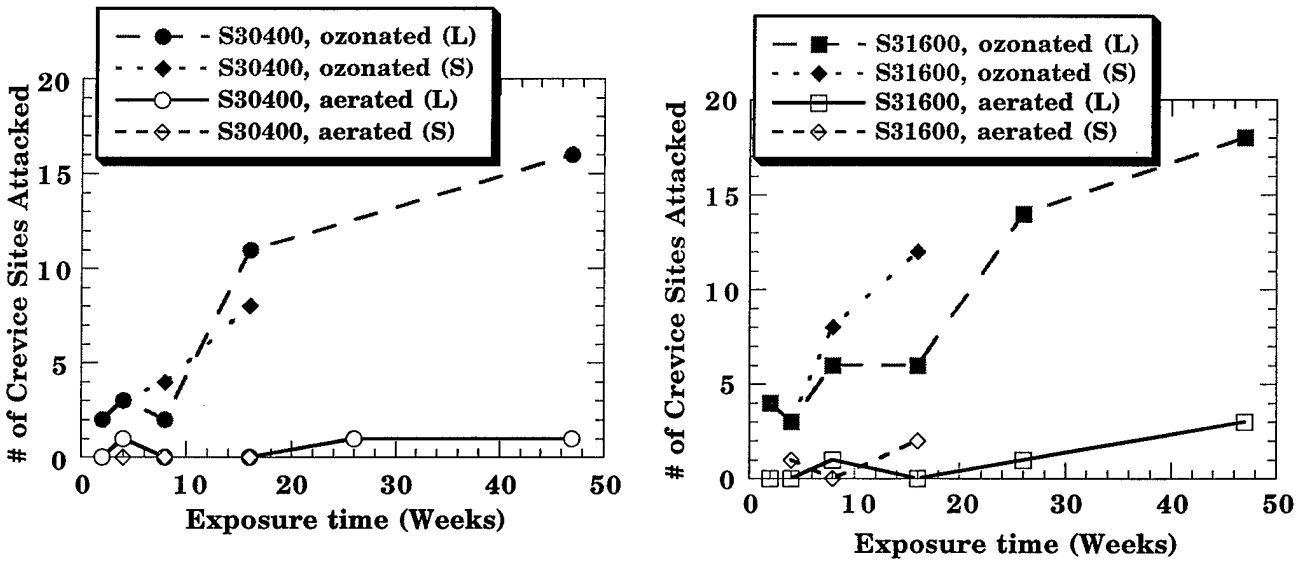

a) b)

Figure 8. Number of crevice sites attacked as a function of time for stainless steels in aerated and ozonated artificial seawater. a) UNS S30400. b) UNS S31600 (S - small cathode area, L - large cathode area)

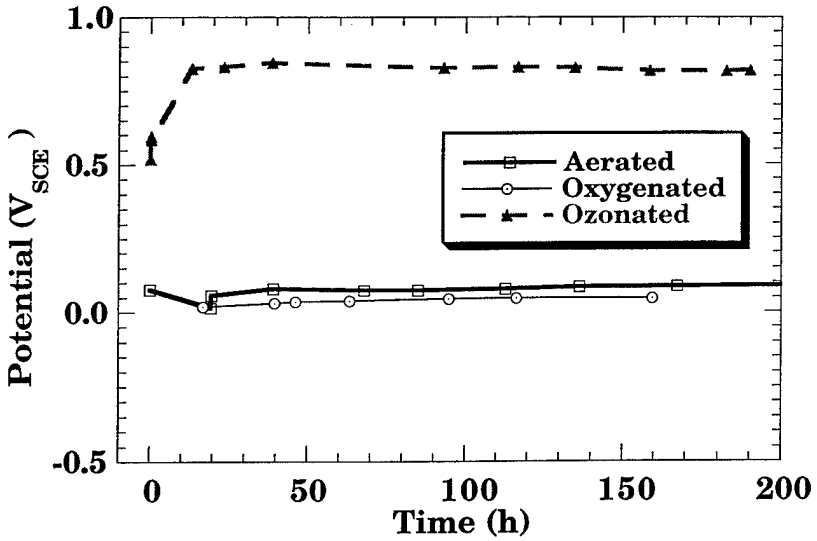

Figure 9. Open circuit potential of uncoupled UNS N08367 electrodes in cathode compartment during compartmentalized cell ZRA experiments.

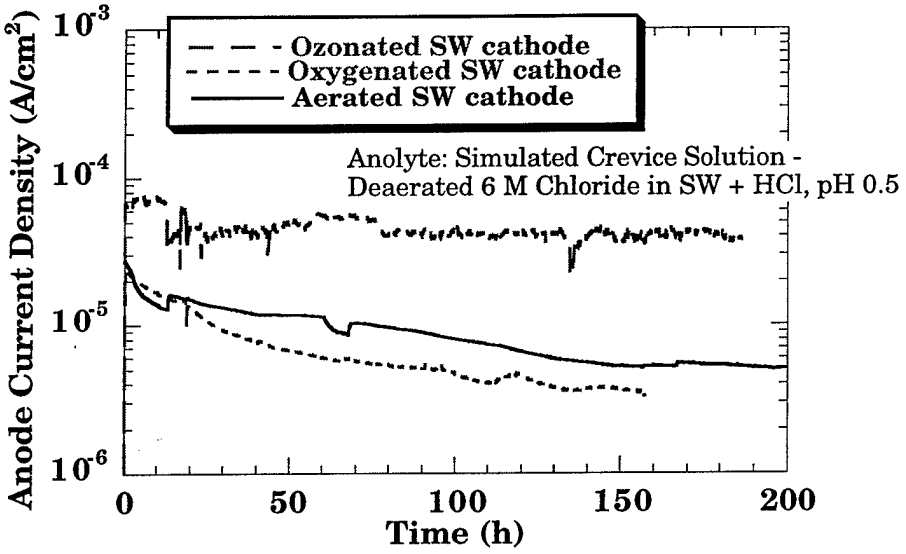

Figure 10. Galvanic current density at the UNS S31600 anode for compartmentalized cell ZRA experiments using a crevice-free anode in simulated crevice anolyte coupled to boldly exposed cathode in artificial seawater, for different cathode cell conditions.

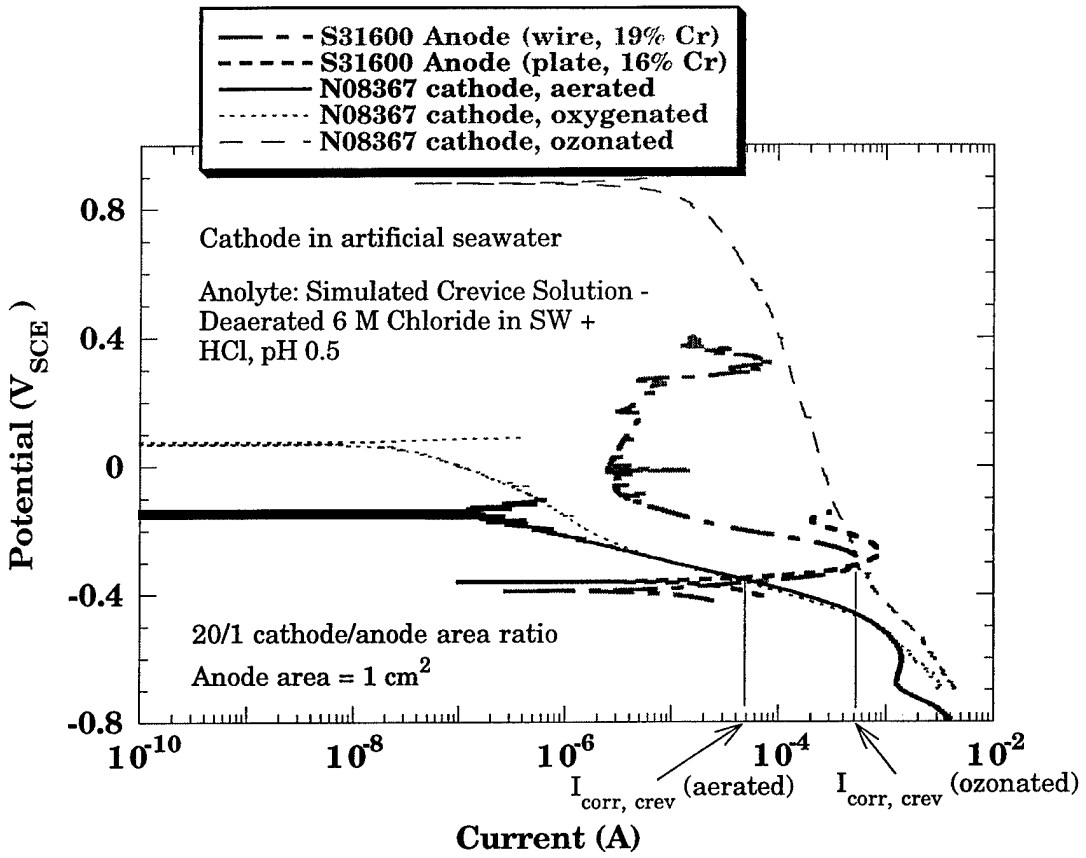

Figure 11. Mixed potential diagram for crevice corrosion of UNS S31600 (16 and 19 wt.% Cr) in simulated crevice anolyte superimposed with cathodic polarization of UNS N08367 in bulk artificial seawater under aerated, oxygenated, and ozonated conditions.

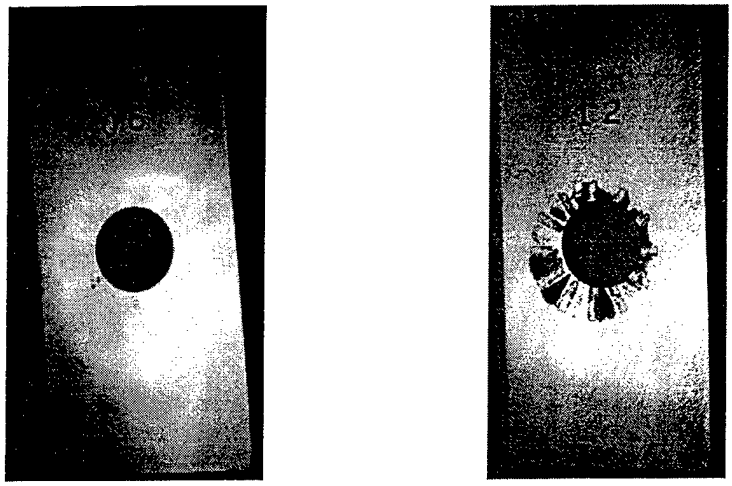

(a) (b)

Figure 12. Small UNS N08367 stainless steel samples, 1.0x2.0 in. (2.5x5.1 cm), exposed for 16 weeks: (a) aerated artificial seawater, (b) ozonated artificial seawater. Representative of the appearance of UNS S32654 and alloy 4565S as well.

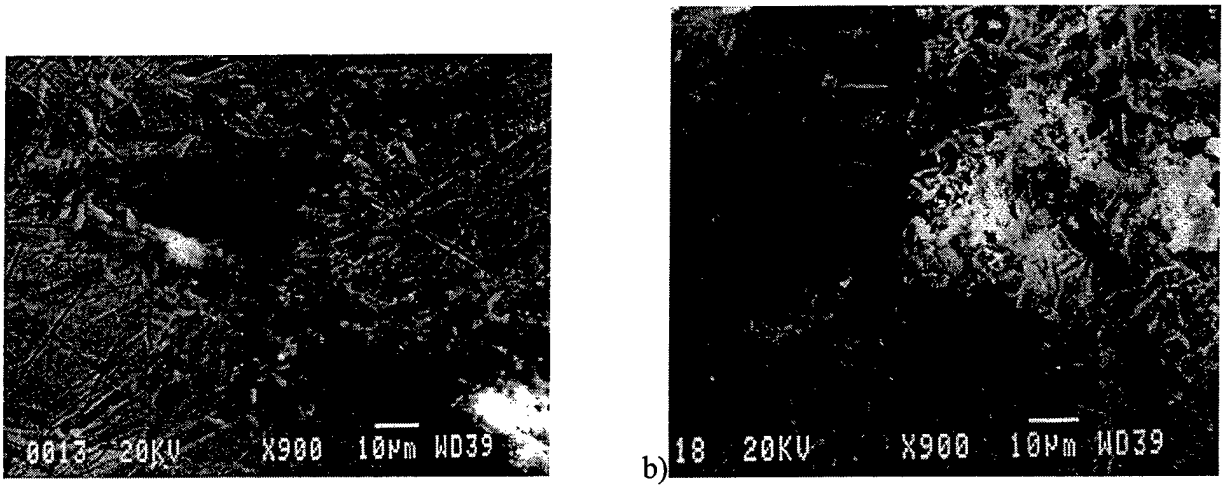

a) b)

Figure 13. Small pits found at the plateau/slot transition of crevice samples exposed for 47 weeks in ozonated seawater. a) UNS N98367 b) UNS S32654

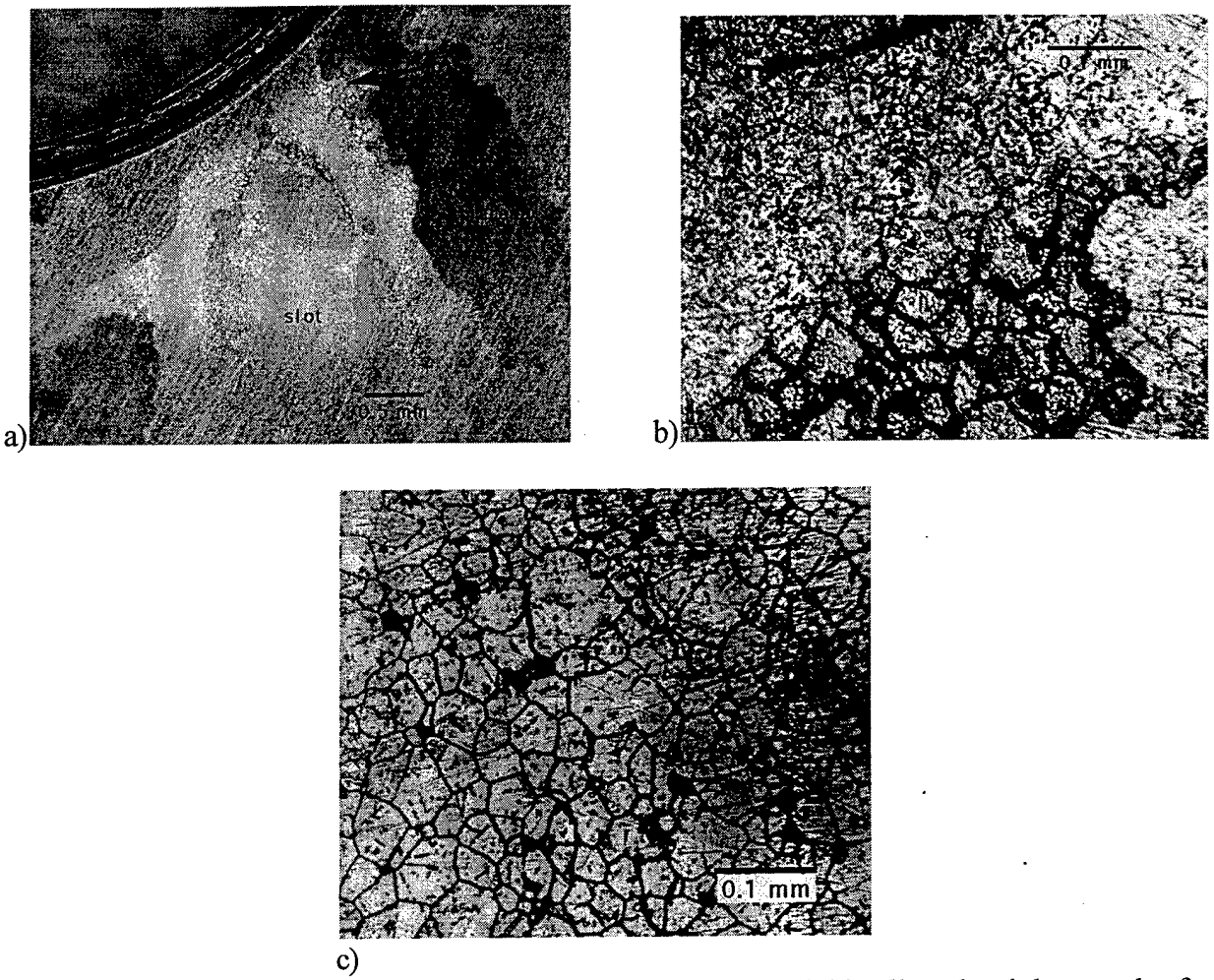

Figure 14. Light micrographs of intergranular corrosion on highly alloyed stainless steels after exposure to ozonated artificial seawater for 16 weeks, corrosion product removed.; a) UNS S32654 in slot and plateau/slot transition. b) High magnification of a) showing intergranular corrosion. c) Intergranular corrosion on UNS N08367 in the center of the slot region.

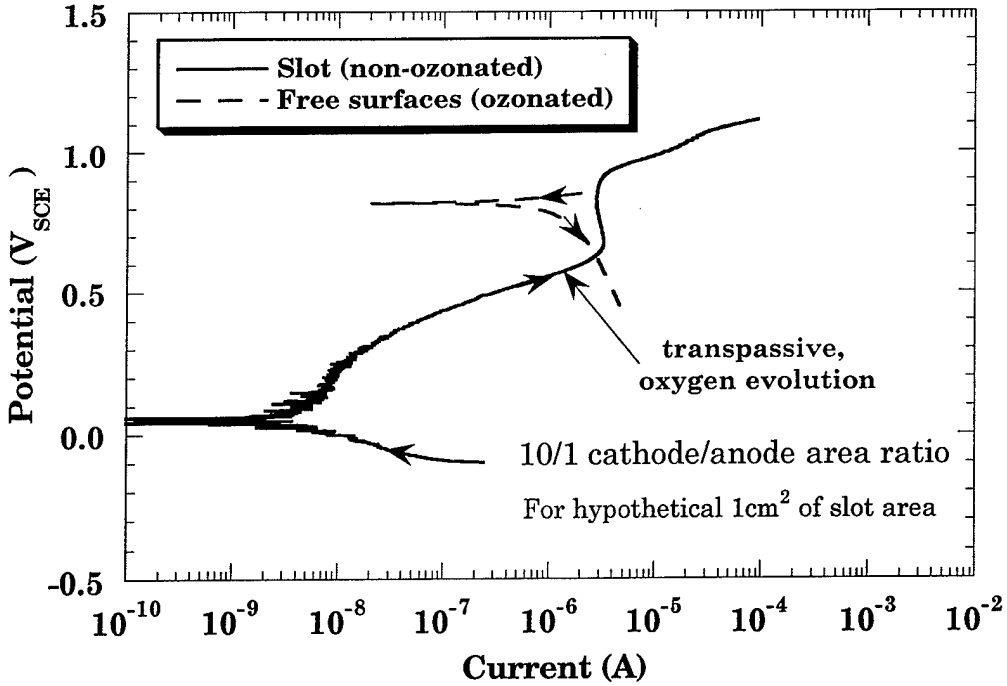

Figure 15. Mixed potential diagram illustrating the couple between the ozonated free surface and the non-ozonated slot region, for UNS N08367. (Scan rate = 1 V/hr)

THE EFFECT OF DISSOLVED OZONE ON THE CORROSION BEHAVIOR OF Ni-Cr-Mo ALLOYS IN ARTIFICIAL SEAWATER

B.E. Brown and D.J. Duquette
Rensselaer Polytechnic Institute
Materials Science & Engineering Department
Troy, New York 12180-3590

ABSTRACT

The effects of ozonated seawater on the corrosion behavior of nickel-chromium-molybdenum alloys C-276, C-22, 625 and 59 (UNS N10276, N06022, N06625, and N06059) were studied and the results were compared with those obtained for aerated solutions. Corrosion rates and crevice corrosion information obtained from plate samples at intervals of 2, 4, 8, 16, 26, and 47 weeks were compared with electrochemical measurements of corrosion potential, linear polarization resistance (LPR), and cyclic polarization curves from concurrently immersed wire samples. It was observed that samples in ozonated seawater, in general, exhibited higher corrosion rates (5-34 μm/yr), as measured by both LPR and weight change measurements, than those exposed to aerated seawater. These relatively low corrosion rates were accompanied by the precipitation of voluminous amounts of black flocculent corrosion product in the ozonated solution, identified as hydrated nickel chlorates formed from dissolved nickel ions in solution. The only adherent corrosion product observed on samples in ozonated solutions is characterized by the presence of a thin oxide film exhibiting interference coloration, which varied from alloy to alloy, and with time of exposure. Creviced samples of alloy C-276 in ozonated seawater showed preferential corrosion at the interface between creviced and uncreviced surfaces, with the creviced surface being completely protected, in contrast to slight pitting damage observed in the crevice region of samples exposed to aerated seawater. Cyclic polarization curves of alloys C-276 and C-22 also suggest increased crevice corrosion susceptibility in ozonated seawater, as indicated by the presence of a hysteresis loop and an increase in the passive current density compared to those observed in aerated seawater. Alloy 690 (UNS N06690) showed severe crevice corrosion in ozonated artificial seawater, indicating the importance of molybdenum as an alloying addition under ozonated conditions.

Keywords: ozone, bromide, hypobromous acid, chlorine, corrosion control, biofouling control, oxidizing biocide, seawater, nickel, nickel-base alloys, molybdenum, transpassivity.

INTRODUCTION

In the early 1900s, ozone was first used to disinfect municipal drinking water in Nice, France.[1] Since then, water treatment by ozonation has been favored over chlorination in Europe because of improved taste, odor control and disinfection. Today, due to the environmental hazards of chlorination byproducts, ozone is currently being used in many fresh water treatment applications in the United States, where only chlorine has been used in the past. These applications include the sterilization of drinking water, treatment of sewage and waste water, algae control in swimming pools, and biofouling control in cooling tower waters.

Although most applications of ozone are in fresh waters, there is a growing number of applications for the use of ozone in seawater. Ozone has already been used successfully in several large aquaria for the treatment of biotoxins in recirculating seawater systems.[2] It is also being investigated for use in preventing biofouling in desalination processes as well as in heat exchangers which use marine waters for cooling.[3]

Ozone is one of the strongest oxidizers used in water treatment. An earlier paper by Wyllie, Brown, and Duquette covers the details of the chemical reactions that occur in ozonated seawater.[4,5] The reaction of ozone with the components of artificial seawater results in the formation of hypobromous acid and bromate ion (Figure 1). Table I shows the redox potentials calculated for different oxidizing conditions, indicating that ozone indeed has a very strong oxidizing effect.

This study focuses on the corrosion behavior of Ni-Cr-Mo alloys in ozonated artificial seawater. The following alloys were studied: C-276, C-22, 625, and 59 (UNS N10276, N06022, N06625, N06059).(1) Alloy 690 (UNS N06690) was included in order to study the effects of molybdenum as an alloying addition.

The Corrosion of Nickel Alloys

Nickel is resistant to general corrosion in seawater, with corrosion rates typically less than 25 µm/y (1 mpy).[6] However, its passive film is not resistant to breakdown by pitting in the presence of chloride ions. Chromium imparts general corrosion resistance to oxidizing environments, and increases the resistance to tarnishing and pitting, but Ni-Cr alloys are still susceptible to localized corrosion. Crevice corrosion resistance is greatly enhanced by molybdenum additions by increasing the resistance to breakdown in the reducing environment created within crevices.[7] For example, corrosion of alloy 625, a Ni-Cr-Mo alloy, was reported to have a corrosion rate of 0.4 µm/y in seawater with no pitting or crevice attack.[8] In the analysis by Streicher,[9] nickel based alloys C-276 and 625 were shown to be immune to crevice corrosion in filtered seawater.

Literature on the effects of water chlorination on Ni-Cr-Mo alloys in artificial seawater show that the crevice corrosion resistance of these alloys increases with increasing molybdenum content: C-276 > 625 > G3 (UNS N06985).[10] In near neutral pH chlorine dioxide bleaching solutions, Ni-Cr-Mo alloys exhibit transpassive general corrosion dissolution but resist crevice corrosion attack.[11] The relative corrosion rates of this transpassive dissolution are such that C-276 (56Ni-16Cr-16Mo-6Fe) < 625 (62Ni-22Cr-9Mo-4Fe) < C-22 (59Ni-21Cr-14Mo-3Fe) < 59 (61Ni-23Cr-16Mo-0.3Fe).[11] From this relationship, it appears that the rates of general corrosion via transpassive dissolution may be

(1) UNS numbers are listed in *Metals and Alloys in the Unified Numbering System*, published by the Society of Automotive Engineers (SAE) and co-sponsored by ASTM.

inversely proportional to iron content of the alloy, or directly proportional to chromium content. It was also found that Ni-Cr-Fe-Mo alloys were susceptible to crevice corrosion, but resistant to transpassive dissolution.[11]

EXPERIMENTAL PROCEDURE

Solutions

Artificial seawater solutions were prepared by adding 1946 g of Forty Fathoms Bio-Crystals Marinemix(2) to 56L of distilled water in a 76-liter tank. This mix is a brand of artificial seawater that contains all of the components of natural seawater, in accordance with ASTM D 1141-90.[12]

Since the bromide ion is the main ion oxidized by ozone in artificial seawater, the initial bromide concentration of each tank was measured using a titration procedure[13] and adjusted by the addition of artificial seawater mix or distilled water, until the bromide concentration was in the range of 800-860 mM/L (63-69 mg/L).

Using a fritted glass bubbler, ozone was bubbled into a tank in combination with oxygen as a carrier gas, at a rate of 0.03 m^3/hr [1 SCFH (standard cubic feet per hour)], while another tank, used as a control, was aerated at the same rate.

The solution in the ozonated tank was measured for changes in pH, as well as concentrations of apparent residual ozone, bromide, hypohalite, and bromate, after 1 day and 1 week of ozonation before samples were immersed. After sample immersion, these values were measured upon removal of test samples. The residual ozone was measured using the Indigo Trisulfonate Method.[14,15] Bromide, hypohalite, and bromate concentrations were measured using a titration procedure.[13,16] The aerated control tank was aerated for 4 days before immersion of samples; the free bromide concentration and pH of this solution were tested prior to sample immersion.

In order to compensate for evaporation and to prevent adverse build-up of byproducts, 6 liters of artificial seawater, in both the aerated and ozonated tank, were extracted weekly and replaced with fresh solution, throughout the course of the experiments.

Ozone Generation and Delivery

Ozone was generated using a combination of an AirSep(3) AS-12 oxygen generator and American Ozone(4) GS2-14 ozone generator. The oxygen generator was set to operate at a pressure of 69 kPa (10 psig) and 55% of maximum output, delivering 90-95% oxygen (nitrogen balance) to the ozone generator at a flow rate of 0.28 m^3/hr (10 SCFH). With the ozone generator operating at a pressure of 21 kPa (3 psig) and at 85% power setting, this produced an ozone concentration of approximately 47 g O_3/m^3 (3.35 wt.% O_3 in 90-95% O_2).

The oxygen/ozone gas mixture was supplied to a stainless steel ball flow meter (0-2 SCFH range), set at 0.03 m^3/hr (1 SCFH), giving a rate of ozone input into the tank of 1.3 g O_3/hr with an

(2) Registered Trademark of Marine Enterprises Intl. Inc.
(3) Registered Trademark of Airsep Corporation
(4) Registered Trademark of American Ozone Systems, Inc.

oxygen input rate of 39 g O_2/hr. From the flow meters, ozone was delivered to each tank via PTFE[5] and Norprene[6] tubing. Only PTFE tubing was used inside the tanks.

Samples

The alloys tested in these experiments, and their chemical compositions, are shown in Table II. Alloy 690 was included in order to study the effects of molybdenum as an alloying addition.

Four basic types of samples were used in these experiments:

1.) Weight Change (plate)
2.) Crevice (plate)
3.) Large Cathode Crevice (plate)
4.) Electrochemical Characterization (wires)

Three weight change and three crevice samples were cut from 0.158 cm (0.063 in) to 0.318 cm (0.125 in) plate into 2.5x5.1 cm (1.0x2.0 in) coupons, in which a 0.95 cm (0.38 in) hole was drilled. In order to determine the affect of different anode/cathode area ratios, seven "large" cathode area crevice samples, measuring 3.8x7.6 cm (1.5x3.0 in), were also cut and a 0.95 cm (0.38 in) hole drilled in the center. The wire sample diameters are listed in Table III. Eight samples of each of the wire alloys were prepared for testing. All samples were ground through 600 grit abrasive, rinsed with distilled water, ultrasonically cleaned in distilled water, and then rinsed again with distilled water.

Sample Fixturing

Three weight change samples of each alloy were suspended in the solution by inserting a glass rod through the holes, using PTFE tubing as spacers between the samples. Crevice samples were assembled between two PTFE crenelated washers, surrounding the hole. The sample and PTFE washers were clamped between Grade-2 titanium washers and secured with a Grade-2 titanium bolt and nut (Figure 2). For purposes of this discussion, the portion of the crenelated PTFE washer which was in contact with the surface of the sample to form the crevice is called the "plateau," while the region separating the plateaus is referred to as the "slot." A PTFE thread was tied to one of the PTFE washers used for each sample; the other end of the thread was tied to a PTFE O-ring for later fixturing. In order to prevent any contact between the sample and the bolt, the bolt was wrapped with PTFE tape prior to assembly. The crevice samples were assembled while submerged in aerated artificial seawater, in order to minimize air pockets and to initiate wetting under the PTFE crenelated washers. After crevice samples were tightened with one and a quarter turns from finger tight, the electrical resistance was checked between the sample and the bolt with a voltmeter. Each sample was re-checked after final removal from the tanks to verify that there had been no electrical contact between the sample and fixture.

Wire samples were bent so that only the cylindrical surfaces of the wires were immersed, in order to eliminate the effects arising from the cut ends of the wires (Figure 3).

Testing

Tests were performed at 1, 2, 4, 8, 16, 26, and 47 weeks following initial immersion. Before any samples were removed or tested in the tanks, the water chemistry was checked.

---

[5] polytetrafluroethylene
[6] Registered Trademark of Norton Performance Plastics Corp.

At each time interval, weight change samples were removed, rinsed in distilled water and allowed to air dry before weighing. After weighing, the samples were photographed, replaced on the glass rods and returned to the tank.

One large cathode area crevice sample of each alloy was removed at each time interval and rinsed in distilled water. The smaller crevice samples were removed at intervals after initial immersion of 4, 8, and 16 weeks. The assembly was then carefully taken apart, and the crenelated washer and fixture archived, if corrosion product was present. The samples were then rinsed in distilled water again and allowed to air dry. The samples were then weighed, photographed, and stored in a dessicator.

At each interval, one wire sample of each alloy was removed from the tank for electrochemical characterization, along with approximately one liter of solution. Care was taken to keep the wire submerged while moving both the wire and tank solution into a one liter cell. A bubbler was placed in the cell, bubbling either air or ozone at a rate of approximately 0.003 m^3/h (0.1 SCFH). Electrochemical measurements of steady state corrosion potential, linear polarization resistance (LPR) and cyclic polarization were performed on the wires. Afterwards, the wires were removed from the cell and the submerged area of the wire surfaces measured.

One wire of each alloy was left in the tank over the course of the entire experiment. At each interval, the steady state corrosion potential and linear polarization resistance of these wires were measured while they remained in the tank.

Linear polarization resistance measurements were collected at a scan rate of 0.6 V/hr for all wire samples. Corrosion rates for all alloys were then calculated from the LPR data based on the assumption that $\beta_a=\beta_c=0.12$. Cyclic potentiodynamic polarization scans of all wires were performed at a rate of 10 V/hr.

RESULTS

Solution Chemistry

In ozonated seawater, voluminous amounts of black flocculent corrosion product precipitated in the tank within 24 hours of the immersion of the samples, and plated onto the glass sides of the tanks. However, fully immersed samples remained free of this corrosion product. The portions of the wire samples below the water line remained free of precipitate, while the sections above the waterline were covered with the precipitate. The precipitate was collected from the ozonated tank, filtered and dried. Examination using energy dispersive spectroscopy (EDS) in the scanning electron microscope (SEM) revealed the presence of primarily calcium, oxygen, chloride, and nickel. Further analysis by x-ray diffraction indicated the presence of calcium oxide, sodium chloride, and identified the precipitate as hydrated nickel chlorate.

Figures 4 and 5 show the typical changes in pH, residual ozone, free bromide, hypohalite, and bromate as a function of time. Values for brominated species are given as percentages of total bromide, which was in the range of 820-880 μM (65-70 mg/L).

After one week of ozonation, the solution chemistry of the artificial seawater reached sTable values. The pH decreased slightly to a value between 8.1-8.2. The residual ozone concentration

stabilized at 0.40 mg/L, and 82% of the total bromide in solution was oxidized to bromate. The amount of free Br^- was 16% of the total bromide in solution, while HOBr and OBr^- were between 0-3%.

After the samples were immersed, a reduction in the amount of residual ozone was observed, occurring over a period of 2 to 8 weeks. This decrease is believed to be due to an increase in ozone demand created by metallic corrosion of the samples, as well as to subsequent oxidation of metal ions by ozone. After the initial decrease, the residual ozone concentration in the tanks recovered to a value of 0.33 mg/L by 16 weeks of sample exposure. These values were lower than the initial concentration prior to sample immersion, reflecting the ozone demand associated with ongoing metallic corrosion. It is important to note that, in the absence of metal corrosion, the ozone concentration would be expected to rise above initial values, due to decreased chemical demand associated with decreasing concentration of unreacted Br^- ion.

After 4 weeks, the concentration of bromide and its byproducts stabilized. In general, the sTable values for each tank were 86% as BrO_3^-, 10% as free Br^- and 2% each as HOBr and OBr^-.

Steady State Corrosion Potential

Electrochemical testing of alloys C-276, C-22, and 625 wires in the tanks showed that the corrosion potential of wires exposed to ozonated artificial seawater is shifted to a sTable value of 0.6-0.8 V noble to the corrosion potential of wires in aerated seawater after 8 to 16 weeks of exposure. Figure 6 shows a typical plot for alloy C-276 representing this behavior. Table IV represents values of steady state corrosion potential measured on wire samples after 47 weeks of exposure.

Corrosion Rates

Figure 7 shows data for the change in corrosion rate with time of alloy C-276, measured from weight change samples, as well as linear polarization resistance measurements. Similar behavior was observed for each of the nickel alloys after exposure to either aerated or ozonated artificial seawater.

Weight Change Samples. Aerated samples showed no visible corrosion damage, with the surface appearing much as when the samples were first immersed. In contrast, the surface of the ozonated samples, with the exception of alloy 690, exhibited colorful thin oxide films which varied in coloration with the alloy type and time of exposure. Preferential corrosion of the weight change samples was observed in ozonated solutions at locations where the samples were in contact with the glass rod and PTFE spacers, indicating that the slight crevice set up by these conditions was sufficient to induce crevice corrosion. After as little as 1 week of exposure, several large nodules of corrosion product were observed on both the longitudinal and transverse edges of the alloy 690 weight change samples.

Samples exposed to aerated conditions gained weight. The corrosion rates for these samples were calculated using the weight change of the sample and a mass balance of oxygen reacting with nickel to form nickel oxide to calculate the amount of nickel in the nickel oxide. In contrast to the aerated condition, the ozonated samples lost weight. This weight loss was used to calculate corrosion rates assuming that the weight of the oxide film on the surface is negligible (due to it showing only interference coloration).

The samples exposed to both ozonated and aerated seawater show a steady decrease in corrosion rate with time, with samples exposed to ozonated solutions having consistently higher corrosion rates after 8 weeks of exposure. Alloys 625 and C-22 exhibited approximately the same general corrosion rates measured from weight change samples as alloy C-276. The corrosion rates of

alloys 690 and 59 in ozonated solutions were initially higher, at 8 μm/y after 1 week of exposure, and decreased only to 3 and 6 μm/y, respectively, at 47 weeks.

Linear Polarization Resistance Measurements. As with the weight change samples, the corrosion rates calculated from LPR measurements on C-276, C-22, and 625 wires were consistently higher in ozonated *vs.* aerated seawater. The corrosion rates calculated in aerated solutions are negligible for all alloys (<0.5 μm/y) over the entire time period. Corrosion rates calculated from LPR measurements in ozonated artificial seawater were initially 7 μm/y for alloy C-276, 9 μm/y for alloy C-22, and 34 μm/y for alloy 625, decreasing to 1.4, 2.1, and 10 μm/y, respectively, after 47 weeks.

Crevice Samples

For all of the alloys and test conditions there were no significant differences between the results for the "small" crevice samples, 2.5x5.1 cm (1.0x2.0 in), and the "large" crevice samples 3.8x7.6 cm (1.5x3.0 in).

For all of the alloys examined, the creviced samples exposed to aerated artificial seawater exhibited a few small pits that initiated after approximately 4 weeks of exposure. Those initiated pits stabilized with no further growth. No other corrosion damage was observed on alloys exposed to aerated artificial seawater.

In ozonated artificial seawater, the exposed surfaces of alloys C-276, C-22, 625, and 59, were covered by a thin oxide which refracted different colorations depending on the alloy and the time immersed. The coloration ranged from yellow-gold-bronze for C-276, 625 and 59 alloys to blue-green for C-22. The slot regions, for the most part, varied from a rainbow effect of oxidized corrosion product to a light brown corrosion product. The exception to this appearance was alloy C-276 which displayed a semi-adherent dark brown corrosion product, and bright metal regions where the corrosion product had spalled, leaving the base metal exposed (Figure 8). The plateaus of the Ni-Cr-Mo alloys, which were in contact with the crenelated washer to form crevices, were uncorroded.

From examinations by SEM and EDS, the dark brown corrosion product in and around alloy C-276 slots was shown to exhibit significant amounts of iron, oxygen, and silicon. The origin of this phenomenon is not understood at this time.

In contrast to the behavior of the Ni-Cr-Mo alloys, alloy 690 exhibited no discoloration of uncreviced surfaces when exposed to ozonated artificial seawater. The slot regions of the ozonated samples exhibited a light blue oxide with some evidence of brown corrosion product. In aerated solutions, a few small pits were observed in some of the crevices. In ozonated solutions, a significant number of crevices exhibited extreme, deep pitting.

From examination by SEM and EDS, the brown corrosion product in the slot region of alloy 690 exposed to the ozonated solution was found to be a semi-adherent film showing high iron and oxygen concentrations. Probing one of the massive pits on an actively corroding plateau (Figure 9), showed pure titanium crystallites, as well as high chromium and silicon concentrations, and a decreased amount of iron compared to the bulk alloy concentration. Trace amounts of niobium were also observed.

Cyclic Potentiodynamic Polarization

Figures 10-12 show 47 week cyclic potentiodynamic polarization (CPP) curves measured after 47 weeks of exposure. These data are representative of all of the time intervals for the alloys after exposure to aerated and ozonated artificial seawater.

Figure 10 shows that the aerated CPP curve of alloy C-276 exhibits both primary and secondary passivity. At a potential of 0.32 V_{SCE} the aerated curve shifts to transpassive behavior, showing very little hysteresis on the return portion of the curve. After 47 weeks, the steady state corrosion potential of the ozonated alloy C-276 was 0.73 V_{SCE}, correlating with the transpassive transition in aerated solutions, indicating that the ozonated wires are in the transpassive region under steady state conditions. The curve for the ozonated condition also shows a very distinct hysteresis loop upon reversal, indicating susceptibility to pitting and crevice corrosion. The formation of a hysteresis loop for the ozonated condition was evident only after 2 weeks of exposure. Examination of the wires after polarization showed that significant amounts of pitting had occurred on the polarized portions of both aerated and ozonated wires below the waterline. Enhanced corrosion was observed at the polarization waterline of the ozonated sample. The appearance of this waterline corrosion was similar to the crevice corrosion observed on ozonated C-276 crevice samples, with the formation of a dark brown corrosion product which spalled away to reveal shiny metallic base metal.

Figure 11 shows that the CPP curves of alloy C-22 exhibit both primary and secondary passivity under aerated conditions, with a transpassive potential of 0.28 V_{SCE}. After 47 weeks, the steady state potential of the ozonated alloy C-22 was 0.73 V_{SCE}. This potential is also noble to the transpassive transition observed in aerated solutions, indicating that the ozonated wires are in the transpassive region under steady state conditions. The polarization curve of the ozonated sample also exhibits a hysteresis loop upon reversal, which was not observed for curves measured before 4 weeks of exposure, or in the aerated solution. After polarization, neither of the wires showed evidence of pitting. However, the ozonated wire did show evidence of corrosion similar to that seen on the crevice samples and wires of alloy C-276.

Alloy 625 (Figure 12) also exhibits a transpassive shift, similar to the other alloys, at a potential of 0.30 V_{SCE}. At 47 weeks, the steady state potential of the ozonated alloy 625 was 0.33 V_{SCE}, just noble to the transpassive transition observed in aerated solutions, indicating that the ozonated wires are in the transpassive region under steady state conditions. Unlike the two other nickel alloy wires, however, alloy 625 shows no evidence of a hysteresis loop in the polarization curves of samples in ozonated solutions at any time period. Examination of the wires after polarization confirmed that there was no evidence of pitting corrosion, or the type corrosion observed on the alloy C-276 or C-22 wires.

DISCUSSION

Solution Chemistry

After the samples were immersed, a decrease in the amount of residual ozone was observed. This decrease is due to an increase in ozone demand created by metallic corrosion of the samples. The ozone is cathodically reduced on the surfaces of the metal samples in order to support the anodic dissolution of the alloys and to establish the passive films. With the onset of sTable passivity the ozone demand was reduced, reflecting the decrease in corrosion rates. The solution pH remained constant, indicating that a continuous supply of ozone did not interfere with the buffering capacity of the solution.

The voluminous, flocculent, black corrosion product observed in the ozonated tank is due to nickel dissolution as Ni^{++} in combination with the reaction products of ozone with the components of the seawater. Based on analyses using energy dispersive spectroscopy (EDS) and x-ray diffraction, the product consists of calcium oxide, sodium chloride, and hydrated nickel chlorate. The chlorate ion in ozonated seawater forms by oxidation of Cl^- -> ClO^- -> ClO_3^- by ozone. Nickel dissolves ionically, reacts with ozone and precipitates as a mixed compound with CaO and NaCl. It is also suspected that the precipitated reaction product contains amorphous $NiO_2 \cdot 2H_2O$, as predicted by the potential-pH diagram[17] at pH 8 - 9 under the oxidizing conditions of ozonated seawater. In the amorphous state, the compound would not be identifiable by x-ray diffraction.

Corrosion Rates

Despite the appearance of the voluminous black product, the corrosion rates calculated from weight change samples and from LPR curves of nickel alloys in ozonated seawater are still very low (< 8 μm/yr and <34 μm/yr, respectively). Comparing the behavior of nickel alloys in ozonated *vs.* aerated seawater, ozone causes an oxide layer to grow with time. This is based on the observation that, in ozonated solutions, the only adherent corrosion product on nickel alloys is characterized by the presence of thin oxide films exhibiting interference type coloration. This oxide varies in apparent thickness from alloy to alloy and with time of exposure to ozonated solutions based on its changes in coloration. Additionally, dissolution is evident in ozonated artificial seawater, based on the green coloration of the solution, indicating dissolution of nickel as Ni^{++}.[17]

Corrosion rates calculated from weight change and LPR measurements showed the same trends of decreasing corrosion rates with time. After 8 weeks of exposure, higher corrosion rates were observed in ozonated *vs.* aerated solutions for all of the alloys examined. Corrosion rates in ozonated solutions calculated from weight change measurements were found to be similar for alloys C-276, C-22 and 625, although values calculated from LPR measurements were found to be slightly higher for alloys C-22 and 625. Although the corrosion rates of nickel alloys in ozonated seawater are slightly higher compared with rates in aerated artificial seawater, and with corrosion rates reported in natural seawater, they are still relatively low.

Potential Shifts

For ozonated solutions, the cathodic reaction is ozone reduction, with the half-cell potential (e) = 1.55 V_{SHE}, while in aerated seawater, the half-cell potential for oxygen reduction at pH 8.2 is 0.73 V_{SHE}. The potential shift observed on the passive alloys is approximately the same (+0.8 to +0.9 V) as the difference between the calculated reduction potentials for ozonated *vs.* aerated seawater, $\Delta e = 1.55 - 0.73 = +0.82$ V from Table I. This correlation indicates that the corrosion potential of the alloys in ozonated seawater is influenced strongly by the presence of ozone rather than by the oxygen carrier gas. At the oxygen content in the feed gas (P_{O_2} = 0.90-0.95 atm), the calculated reduction potential for oxygenated seawater is 0.75 V_{SHE}, only 0.02 V noble to the aerated seawater value. Accordingly, higher oxygen concentrations in ozonated seawater, alone, are not the cause of the corrosion potential shifts.

Crevice Corrosion

Cyclic potentiodynamic polarization testing of alloy C-276, C-22, and 625, show that these alloys are transpassive in ozonated seawater. The open circuit corrosion potentials in ozonated seawater are in a transpassive region of the polarization curves when superimposed on the aerated CPP data, after as little as 4 weeks exposure to ozonated seawater. In aerated seawater, CPP testing indicates that these alloys are resistant to crevice corrosion; the CPP curves do not show breakdown or

hysteresis. However, pitting is observed on the surface of alloy C-276 wires after polarizing in aerated artificial seawater.

After 8 weeks of exposure to ozonated seawater, significant differences are observed in the CPP curves of alloy C-276 and C-22 when compared to the aerated data. The secondary passive regions are more pronounced and a defined transpassive potential as well as hysteresis are clearly evident upon reversal of the scan. The CPP data for alloy 625 is the exception to this; there is no hysteresis observed under ozonated *vs.* aerated conditions. Examination of the alloy C-276 and C-22 wire samples exposed to ozonated solutions after they had been polarized showed the appearance of corrosion similar to the crevice corrosion observed on ozonated alloy C-276 crevice samples, with the formation of a dark brown corrosion product which spalled away to reveal shiny metallic base metal. The alloy C-22 wires exhibited only very small regions of this type of corrosion over the surface of the wire, with no evidence of pitting. In the case of alloy C-276 wires, this corrosion occurred at the waterline, in addition to extensive pitting on the wire surface that was submerged. The results obtained from CPP curves of these alloys were supported by the observation of enhanced corrosion of alloys C-276 and C-22 weight change samples in the slight crevice area formed by contact with the glass rod and PTFE spacers, after 8 weeks of exposure to ozonated seawater.

In both aerated and ozonated seawater, the nickel alloys containing molybdenum show resistance to classical crevice corrosion. The exception to this is the case of alloy 690 in ozonated seawater, which does exhibit classical crevice corrosion; the initially passive surface actively corrodes under the tight crevice plateaus. In aerated seawater, crevice corrosion was also noted for alloy 690, although to much lower extent. Alloy 690 does not contain molybdenum, which is necessary for resistance of nickel alloys to the reducing acidified chloride environment that develops in tight crevices.[7] It may be noted that the Ni-Cr-Fe alloys which do not contain molybdenum, such as alloy 690, are usually selected for resistance to oxidizing conditions rather than for resistance to crevice corrosion in seawater.

The significance of molybdenum as an alloying element for reducing crevice corrosion susceptibility is clearly demonstrated by the results for alloy 690. Although the molybdenum-bearing nickel alloys in this test program show resistance to classical crevice corrosion, they do exhibit a different form of localized corrosion behavior. The plateau creviced regions of the samples exposed to ozonated seawater are uncorroded, exhibiting resistance to reducing environments characteristic of molybdenum containing alloys. However, the corrosion morphology of the slot regions exhibit the formation of a dark brown corrosion product. This behavior indicates that a differential oxidation cell develops between the high ozone activity at the bulk surfaces and the low ozone activity in the slot regions of the creviced washers.

CONCLUSIONS

1.) In the case of nickel alloys, ozonation polarizes the alloys into the transpassive region of the polarization curves.

2.) For all the non-creviced alloys, the material loss that occurs in ozonated artificial seawater appears to be sufficiently low such that general corrosion is not considered to be a problem.

3.) Creviced nickel alloys containing molybdenum did not exhibit classical crevice corrosion behavior. Preferential corrosion occurred at the interfacial regions, leaving the actual crevice (plateau) protected due to differential oxidation. This crevice corrosion, however, is not severe.

4.) The absence of molybdenum in a nickel alloy, as in the case of alloy 690, however, displays normal crevice corrosion behavior which was on the order of severity of that seen with the low molybdenum stainless steels.[5]

ACKNOWLEDGMENTS

The authors are grateful for the support of the Office of Naval Research, and Dr. A.J. Sedriks, under contract N00014-90-J-1439.

REFERENCES

1. P. C. Singer, Journal of American Water Works 82, Oct. (1990) p. 77-88.
2. D. L. LaBonne, "Ozonation of Marine Mammal Pool Waters," (Baltimore, MD: National Aquarium in Baltimore, 1990).
3. R. Sugam, J. H. Singletary, W. A. Sandvik and C. R. Guerra, Ozone Science and Engineering 3, (1981) p. 95-107.
4. W. E. Wyllie II, B. E. Brown and D. J. Duquette, "Ozone in Seawater, Part 1: Chemistry, Part II: Corrosion of Metals," CORROSION/95, paper no. 269 (Houston, TX: NACE International, 1995).
5. W. E. Wyllie II, B. E. Brown and D. J. Duquette, "Interim Results on the Corrosion Behavior of Engineering Alloys in Ozonated Artificial Seawater," Office of Naval Research, Report 2, Contract No. N00014-94-1-0093, March, 1996.
6. M. G. Fontana, Corrosion Engineering, 3rd Ed. (New York: McGraw-Hill, Inc., 1986), p. 374.
7. H. H. Uhlig and R. W. Revie, Corrosion and Corrosion Control (New York: John Wiley & Sons, 1985).
8. F. W. Fink and W. K. Boyd, The Corrosion of Metals in Marine Environments (Colombus, OH: Bayer & Co., Inc., 1970).
9. M. A. Streicher, Materials Performance 22, May (1983) p. 37-50.
10. R. S. Lillard, M. P. Jurinski and J. R. Scully, Corrosion 50, 4 (1994) p. 251-265.
11. D. A. Wensley and D. C. Reid, "Transpassive Dissolution of Nickel-Base Alloys," CORROSION/93, paper no. 433 (Houston, TX: NACE International, 1993).
12. ASTM D 1141-90, "Standard Specification for Substitute Ocean Water," (Philadelphia, PA: ASTM, 1990).
13. K. Grasshoff, Verlag Chemie (1976) p. 324.
14. H. Bader and J. Hoigne', Water Research 15 (1981) p. 449-456.

15. H. Bader and J. Hoigne, "Colorimetric Method for the Measurement of Aqueous Ozone based on the Decolorization of Indigo Derivatives," Ozonation Manual for Water and Wastewater Treatment, W. J. Masschelein (Chichester: John Wiley & Sons, 1982) 169-172.
16. W. R. Haag, Water Research 15, (1981) p. 937-940.
17. M. Pourbaix, Atlas of Electrochemical Equilibria in Aqueous Solutions (Houston, TX: National Association of Corrosion Engineers, 1974).
18. W. R. Haag and J. Hoigné, J. Environ. Sci. Technol. 17, 5 (1983a) p. 261-267.

Table I. Reduction potentials for various oxidizing reactions.

Redox Couple	e^0 (V_{SHE})	Nominal conditions in artificial seawater, pH 8.2	e (V_{SHE}) at nominal conditions
O_3/O_2	2.08	Ozonated, $p(O_3)$ = 0.024 atm	1.55
$HOCl/Cl^-$	1.48	Chlorinated, [HOCl] = 25 mg/l	1.15
$HOBr/Br^-$	1.33	Brominated, [HOBr] = 25 mg/l	1.08
O_2/OH^-	1.23	Oxygenated, $p(O_2)$ = 0.95 atm	0.75
O_2/OH^-	1.23	Aerated, $p(O_2)$ = 0.2 atm	0.73

Table II. Chemical composition (wt.%) based on mill analyses of nickel-base alloy plate samples used for seawater immersion tests.

	C	Cr	Fe	Mn	Mo	Ni	P	S	Si	Other
Alloy 625 (UNS N06625)	0.02	21.71	3.97	0.08	8.82	bal.	0.007	0.001	0.09	0.27 Ti, 3.41 (Ta+Nb)
Alloy 276 (UNS N10276)	0.003	16.02	6.27	0.45	15.89	bal.	0.011	<0.002	0.04	1.83 Co, 0.16 V, 3.51 W
Alloy 22 (UNS N06022)	0.004	20.65	2.61	0.21	14.08	bal.	0.004	<0.001	0.03	0.06 Cu, 0.11 Co, 0.02 V, 3.29 W
Alloy 59 (UNS N06059)	0.005	22.65	0.29	0.15	15.6	bal.	0.002	0.002	0.03	0.03 Co, 0.14 V, 0.08 W
Alloy 690 (UNS N06690)	0.01	29.10	10.26	0.42	-	bal.	-	0.003	0.30	0.29 Ti, 0.22 Al

Table III. Diameters of wire alloys tested.

Alloy	Wire Diameter	
	(cm)	(in)
C-276	0.159	0.0625
C-22	0.239	0.0940
625	0.159	0.0625

Table IV. Steady state corrosion potentials of wire samples after 47 weeks of exposure.

Alloy	Steady State Corrosion Potential (V_{SHE})	
	Aerated	Ozonated
C-276	0.014	0.731
C-22	0.054	0.730
625	0.171	0.327

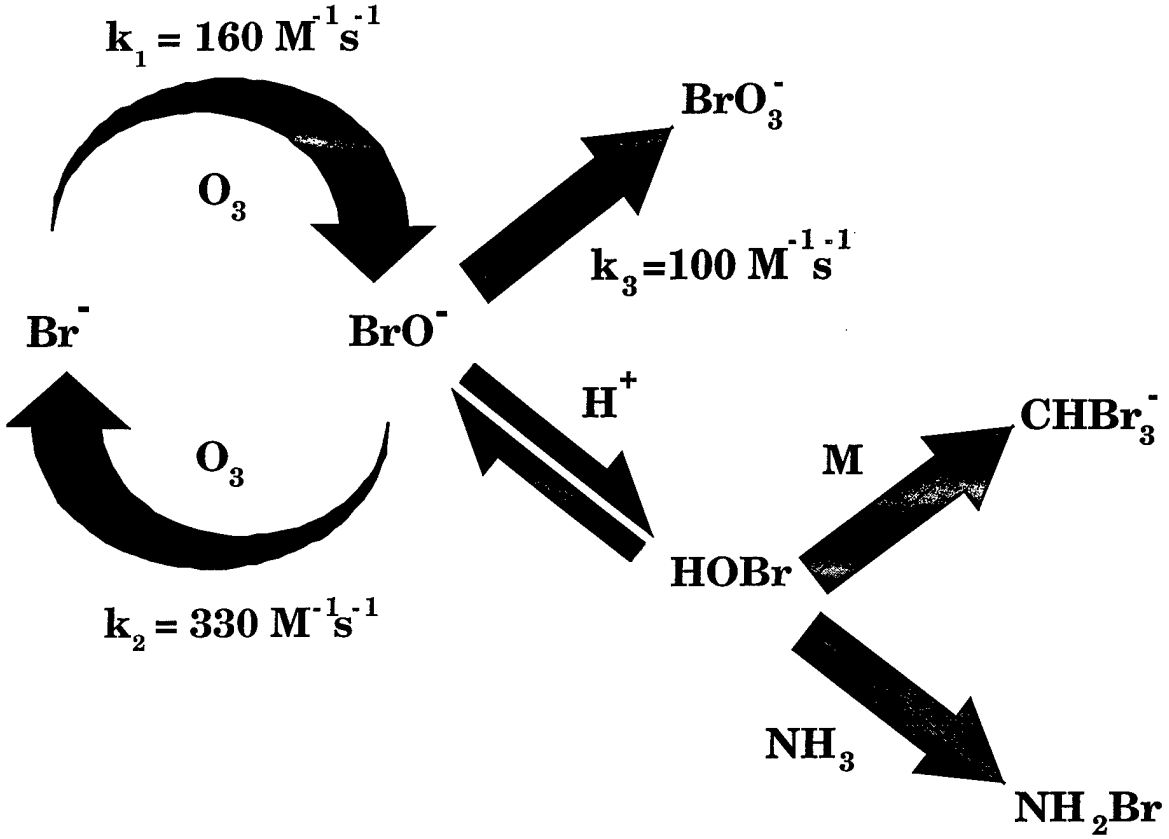

Figure 1. Reaction cycle caused by the ozonation of bromide in seawater.[18]

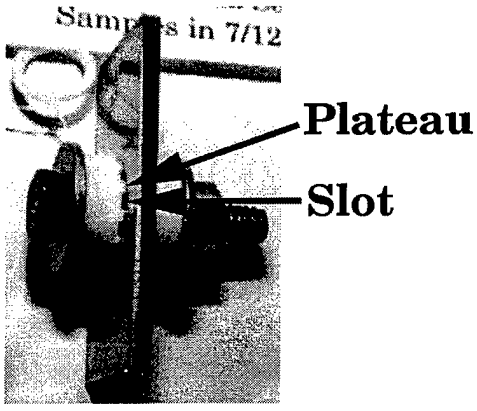

Figure 2. Crevice assembly.

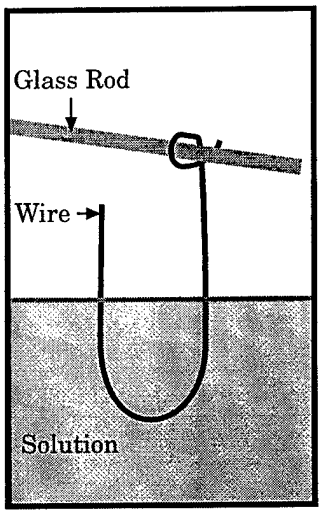

Figure 3. Wire schematic.

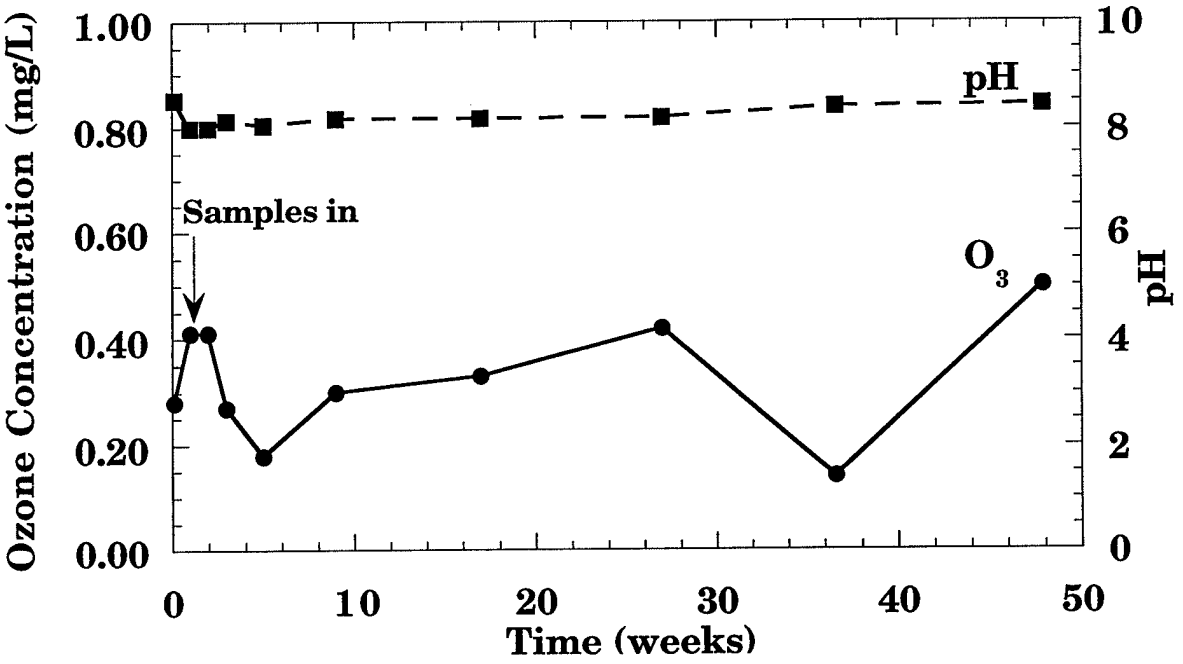

Figure 4. Change in pH and measured residual ozone concentration with time, for ozonated artificial seawater containing nickel alloys.

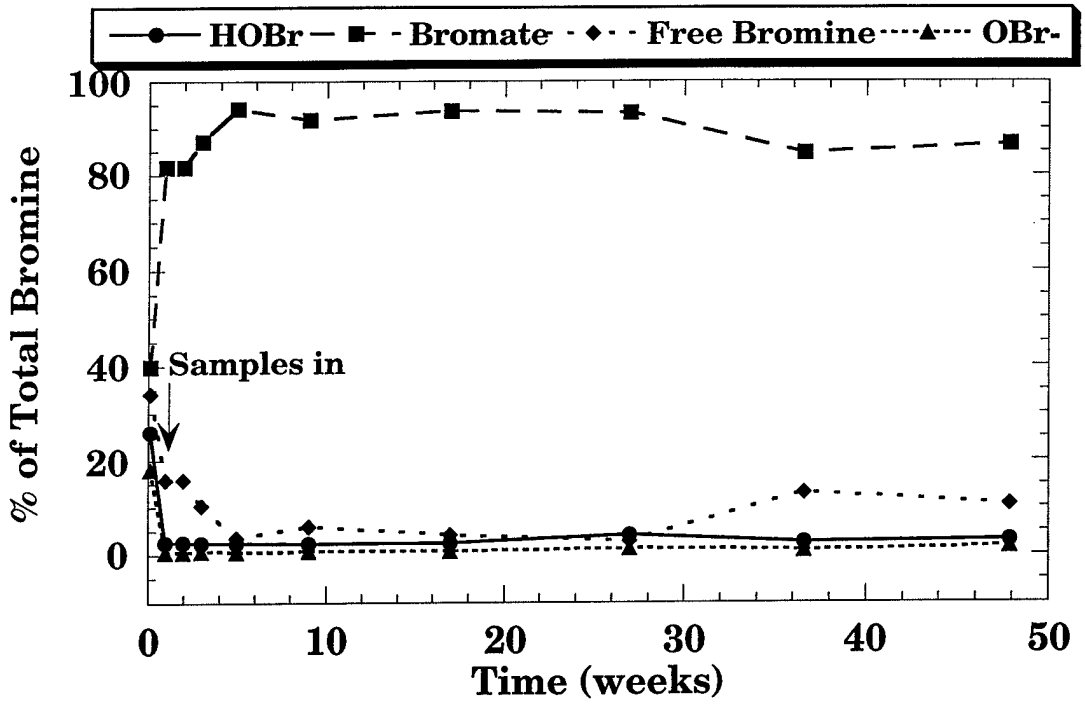

Figure 5. Change in concentration of bromide, hypohalites, and bromate with time, for ozonated artificial seawater containing nickel alloys.

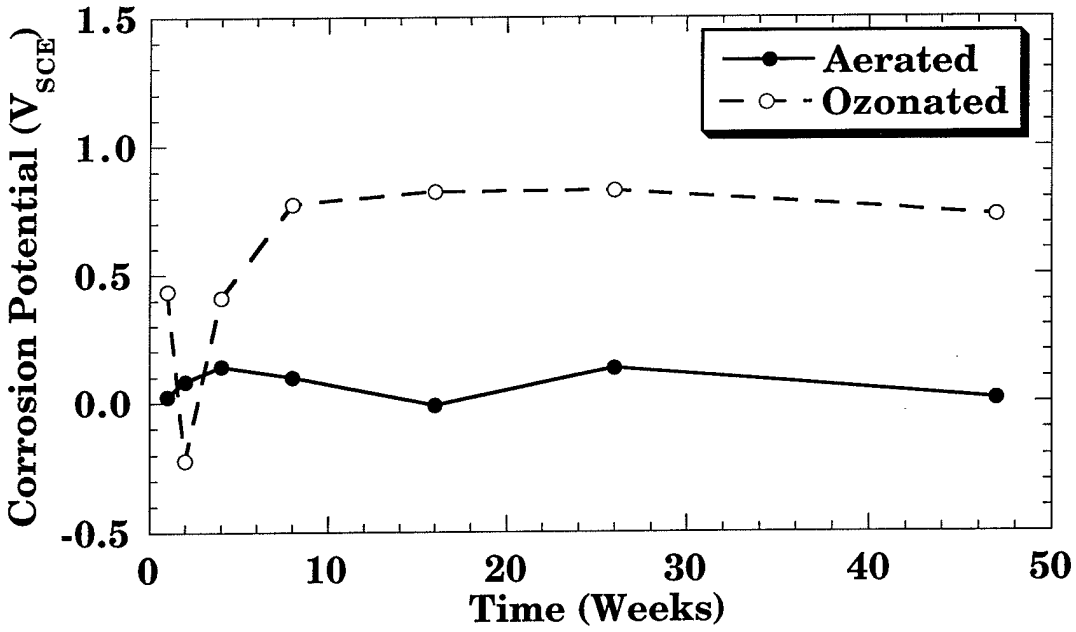

Figure 6. The steady state corrosion potential of alloy C-276 wire representing typical behavior of Ni-Cr alloys in ozonated and aerated artificial seawater.

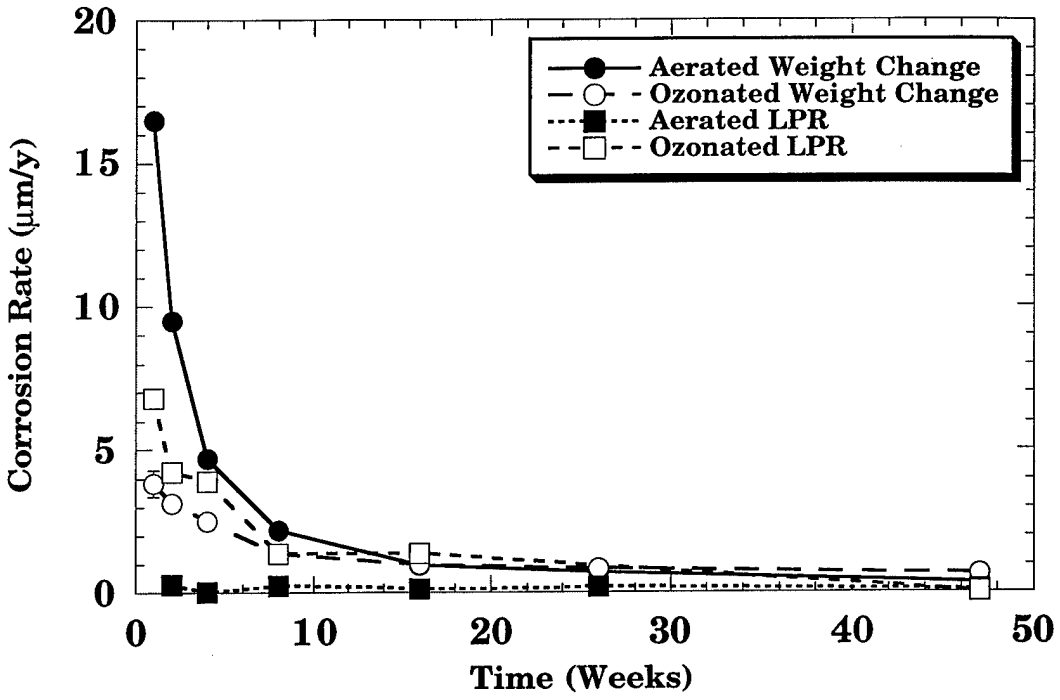

Figure 7. Corrosion rate as a function of time calculated from both weight change samples and linear polarization resistance measurements of alloy C-276 exposed to aerated and ozonated artificial seawater.

(a)

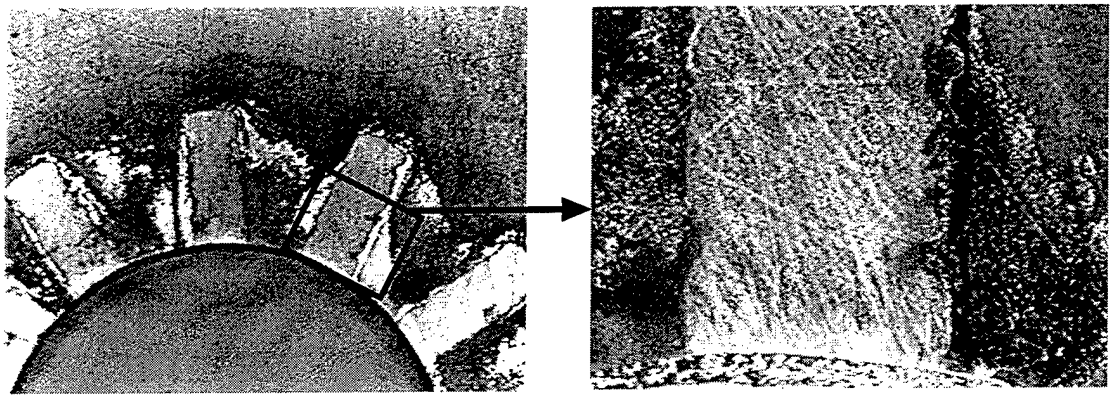

7.6x **26x**

(b) (c)

Figure 8. (a) Small alloy C-276 crevice sample, 2.5x5.1 cm (1.0x2.0 in), after 8 weeks of exposure to ozonated artificial seawater.
(b) Creviced surface of the sample at 7.6x. Shiny metallic regions are observed where dark brown corrosion product had spalled away in the slot region.
(c) Magnified view of the boxed area at 26x, showing shiny metallic regions on either side of plateau.

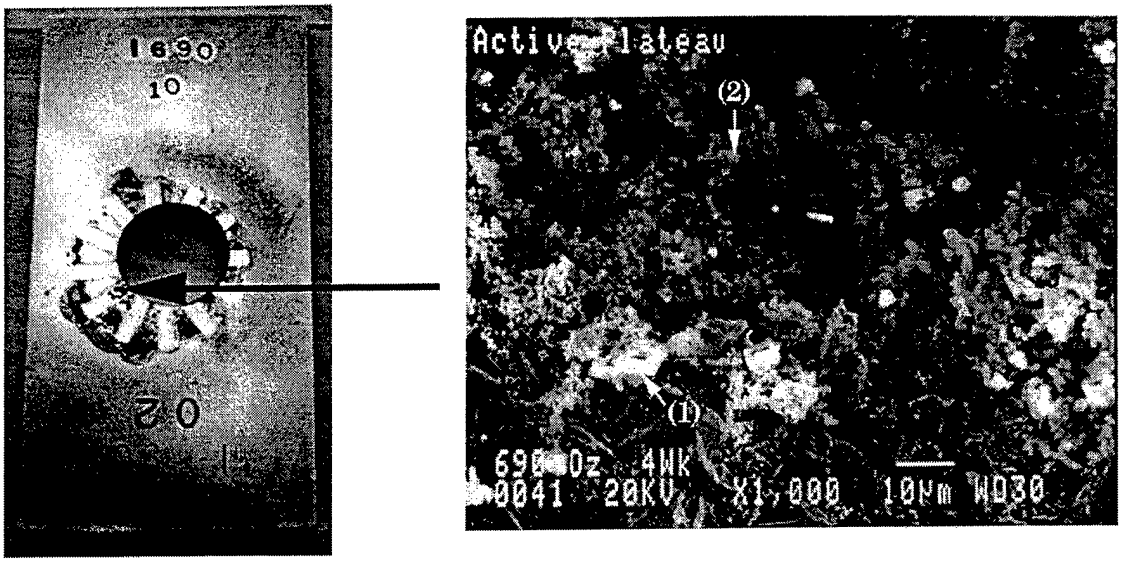

Figure 9. Small alloy 690 crevice sample, 2.5x5.1 cm (1.0x2.0 in), after 4 weeks of exposure to ozonated artificial seawater. SEM photograph on the right depicts an active pit on a plateau. EDS spot analysis of area (1) showed a pure titanium crystallite, while area (2) showed high amounts of titanium, chrome, silicon, and a trace of niobium.

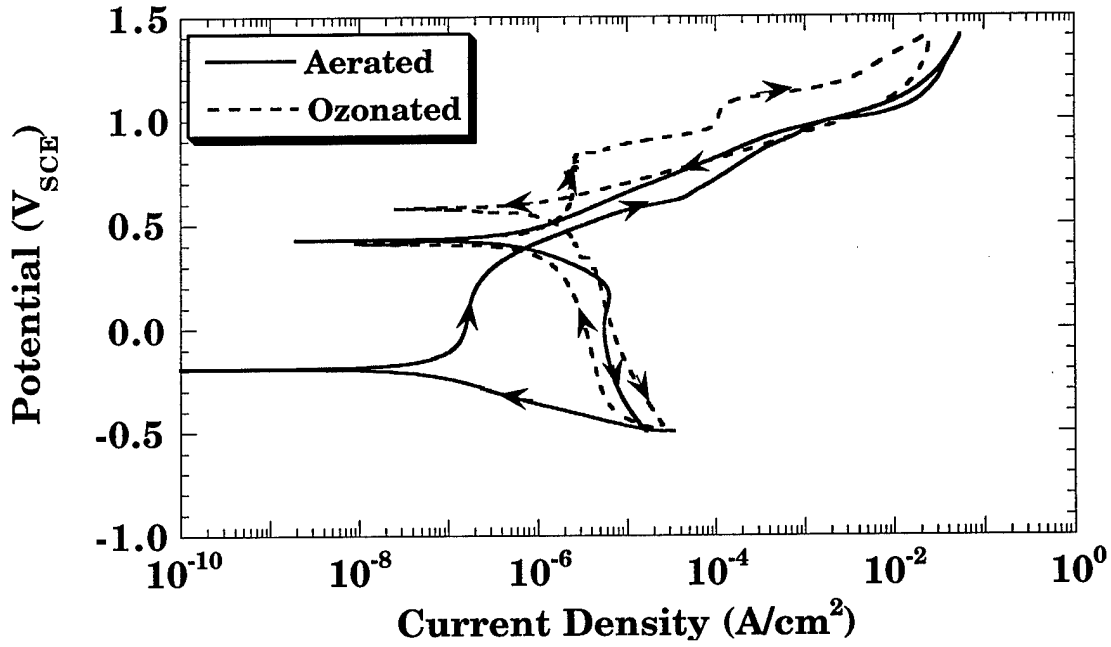

Figure 10. A comparison of the polarization curves of alloy C-276 wires exposed to aerated and ozonated artificial seawater for 47 weeks.

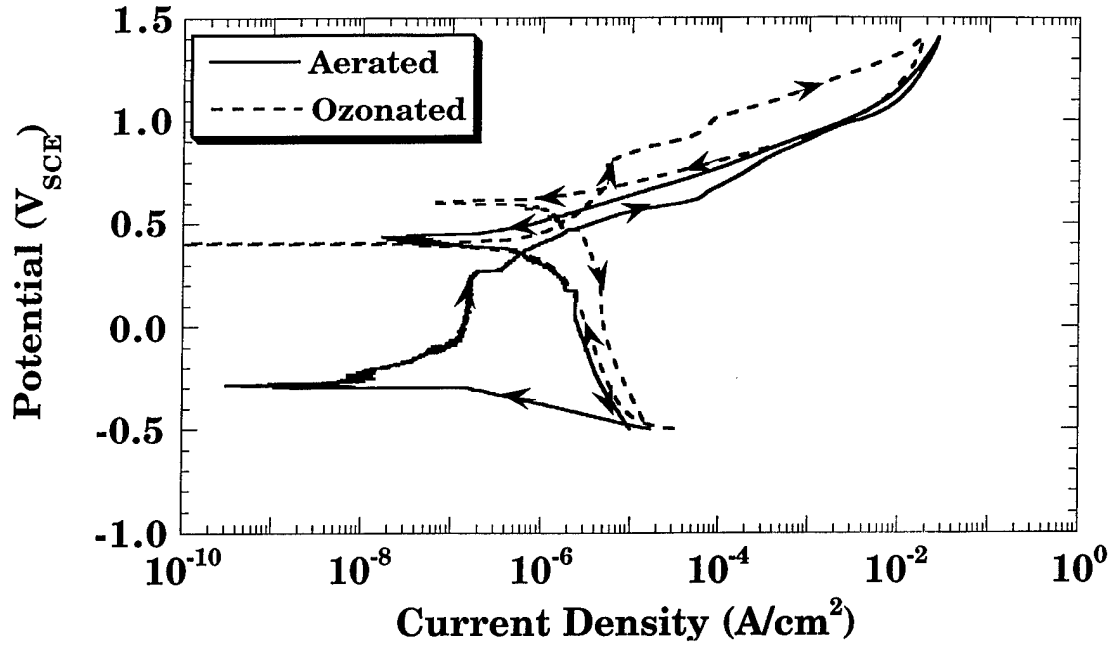

Figure 11. A comparison of the polarization curves of alloy C-22 wires exposed to aerated and ozonated artificial seawater for 47 weeks.

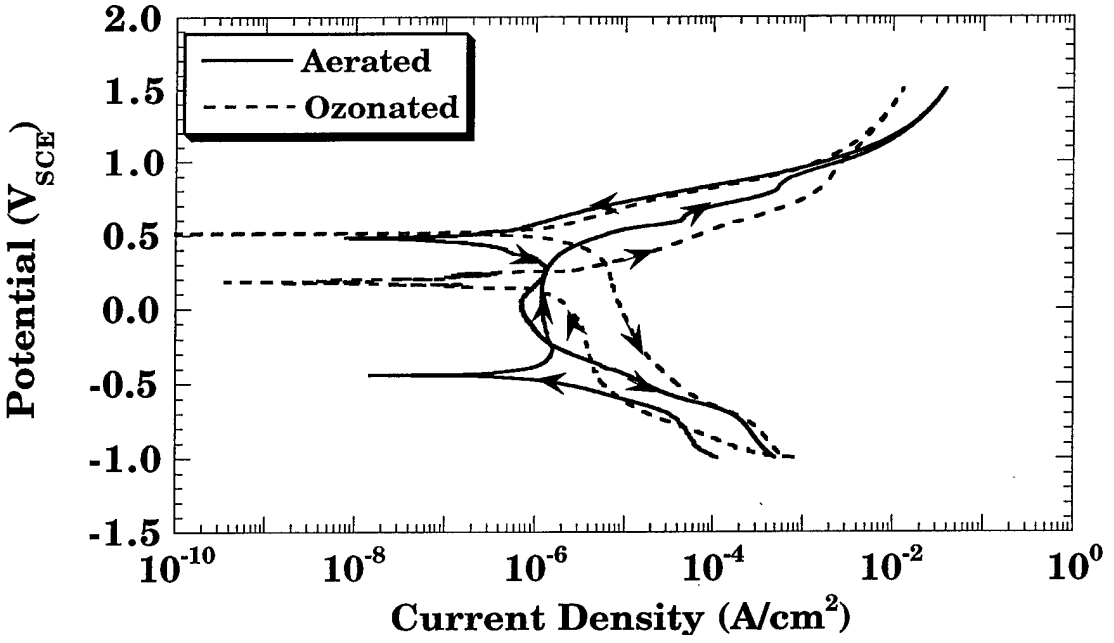

Figure 12. A comparison of the polarization curves of alloy 625 wires exposed to aerated and ozonated artificial seawater for 47 weeks.